

# Explicit formulas for forced convection in a shrouded longitudinal-fin heat sink with clearance

Toby L. Kirk 1 and Marc Hodes 2

Corresponding author: Toby L. Kirk, t.l.kirk@soton.ac.uk

(Received 11 December 2024; revised 15 May 2025; accepted 17 June 2025)

We consider laminar forced convection in a shrouded longitudinal-fin heat sink (LFHS) with tip clearance, as described by the pioneering study of (Sparrow, Baliga & Patankar 1978 J. Heat Trans. 100). The base of the LFHS is isothermal but the fins, while thin, are not isothermal, i.e. the conjugate heat transfer problem is of interest. Whereas Sparrow et al. numerically solved the fully developed flow and thermal problems for a range of geometries and fin conductivities, we consider the physically realistic asymptotic limit where the fins are closely spaced, i.e. the spacing is small relative to their height and the clearance above them. The flow problem in this limit was considered by (Miyoshi et al. 2024, J. Fluid Mech. 991, A2), and we consider the corresponding thermal problem. Using matched asymptotic expansions, we find explicit solutions for the temperature field (in both the fluid and fins) and conjugate Nusselt numbers (local and average). The structure of the asymptotic solutions provides further insight into the results of Sparrow et al.: the flow is highest in the gap above the fins, hence heat transfer predominantly occurs close to the fin tips. The new formulas are compared with numerical solutions and are found to be accurate for practical LFHSs. Significantly, existing analytical results for ducts are for boundaries that are either wholly isothermal, wholly isoflux or with one of these conditions on each wall. Consequently, this study provides the first analytical results for conjugate Nusselt numbers for flow through ducts.

Key words: convection, microscale transport, convection in cavities

<sup>&</sup>lt;sup>1</sup>School of Mathematical Sciences, University of Southampton, Southampton SO17 1BJ, UK

<sup>&</sup>lt;sup>2</sup>Department of Mechanical Engineering, Tufts University, Medford, MA 02155, USA

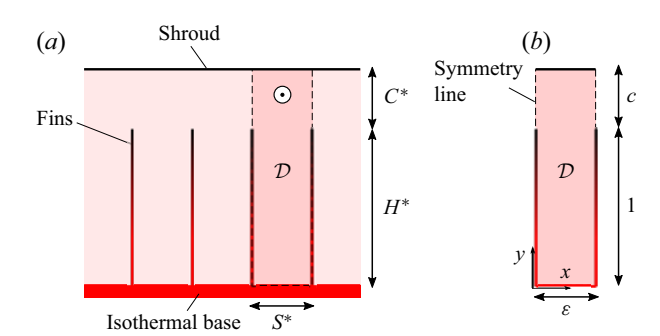


Figure 1. Schematic cross-section of the periodic fin array (a) considered here and by Sparrow et al. (1978); and the dimensionless single period domain  $\mathcal{D}(b)$ .

#### 1. Introduction

Heat sinks are ubiquitous in modern computing and telecommunications hardware. More generally, they are an enabling technology in the thermal management of all electronics and elsewhere. When the flow is unidirectional, generally the fins on them are nearly rectangular in cross-section, in which case the heat sink is referred to as a longitudinal-fin heat sink (LFHS). LFHSs are manufactured by various methods (extrusion, skiving, machining, etc.), each imposing constraints on, e.g. minimum fin spacing and thickness, maximum fin height-to-spacing ratio, materials and cost (Iyengar & Bar-Cohen 2007). Both air-cooled LFHSs (say, in a laptop) and water-cooled ones (say, in a 'cold plate' attached to a central processing unit, CPU, in a server blade) are common. The materials of LFHSs are most commonly aluminium or copper, although the former is incompatible with water.

The foundational study on laminar (forced) convection in an LFHS was published by Sparrow, Baliga & Patankar (1978). They considered fully developed flow and heat transfer and allowed for tip clearance between the top of the fins and an adiabatic shroud, but not for bypass flow around the sides of the LFHS. Viscous dissipation was assumed negligible and thermophysical properties were considered to be constant. Their key results pertained to an isothermal base, a valid assumption in modern applications when, as is common, the fins are attached to a vapour chamber. A key assumption invoked by Sparrow *et al.* (1978) was that, geometrically, the fins were considered to be vanishingly thin, and they neglected heat sink edge effects. Consequently, the fluid domain in one period was rectangular and, due to symmetry, its width was half the fin spacing as per figure 1. The dimensional fin spacing was  $S^*$ , the fin height  $H^*$  and the clearance  $C^*$ . Their hydrodynamic results were provided via tabulations of the Poiseuille number (Po, or product of the friction factor and Reynolds number) as a function of the ratio of the fin-spacing-to-height ratio ( $\varepsilon = S^*/H^*$ ) and fin-clearance-to-height ratio ( $c = C^*/H^*$ ).

In the thermal problem, Sparrow *et al.* (1978) assumed that the Biot number based on the thickness of the fins was small; therefore, temperature varied only along its height. Importantly, the conjugate thermal problem (where the convection problem is coupled to a conduction problem in the fin) was solved by matching temperature and balancing the net heat conduction rate along a differential height of the fin with the heat rate into the fluid along the fin–fluid interface. In addition, heat transfer between the prime surface (between fins) and the fluid was captured. The local Nusselt numbers (Nu) along the fin and prime surface were provided as a function of non-dimensional distance x (along the prime surface) or y (along the fin),  $\varepsilon$ , c and a dimensionless fin conduction parameter  $\Omega$ 

$$\Omega = \frac{k_f}{k} \frac{t^*}{2H^*},\tag{1.1}$$

where  $k_f$  is the thermal conductivity of the fin and k is that of the fluid, with  $t^*$  the thickness of the fin. The fin becomes isothermal as  $\Omega \to \infty$ . They further provide a Nusselt number averaged over the prime surface and fin,  $\overline{Nu}$ , that is independent of x and y, and a key engineering parameter. A key conclusion of Sparrow et al. (1978) was that the ubiquitous assumption of a constant heat transfer coefficient along the prime surface and fin is generally invalid. Alas, it remains common today. In a subsequent and related study, Sparrow & Hsu (1981) relaxed the assumptions of the fins being vanishingly thin in the hydrodynamic problem and the fin temperature being constant across its width. (Axial conduction remains neglected in the fin and the fluid as in our own analysis to follow). The effects on the Poiseuille number were modest in the parametric ranges considered for realistic heat sink geometries. Moreover, it was shown that the adiabatic fin tip assumption compares well with the case where convection from the fin tip is captured because this assumption causes a marked increase in heat transfer near the tip.

Karamanis & Hodes (2016), albeit restricting their attention to fully shrouded LFHSs (i.e. c = 0), discuss relevant studies subsequent to those by Sparrow *et al.* (1978), including representative ones pertaining to the conjugate problem. Additionally, they provide a procedure using the formulation by Sparrow *et al.* (1978) to find the unique combination of fin spacing, thickness and length which minimise the thermal resistance of an LFHS for a prescribed pressure drop driving the flow through it, fin height and fluid-to-solid thermal conductivity ratio. The engineering parameters Po and  $\overline{Nu}$  suffice for this. Dense tabulations of them relevant to the optimisation of the geometry of LFHSs when the fluid-to-solid thermal conductivity ratio is that of air-to-copper, air-to-aluminium, water-to-copper and water-to-silicon are provided by Karamanis (2015).

Subsequent research by Karamanis & Hodes (2019a), again for the fully shrouded case  $(C^* = 0)$ , considered simultaneously developing flow through an LFHS and relaxed the low Biot number assumption, thereby accounting for temperature variation also across the fin's thickness. Then, the Poiseuille number depends explicitly on the fin thicknessto-height ratio  $(t = t^*/H^*)$ , as well as an additional parameter, i.e.  $L^+ = L^*/(D_h Re_{D_h})$ as per numerical results by Curr, Sharma & Tatchell (1972) and, subsequently, many others (Shah & London 1978). Here  $L^*$  is the streamwise channel length, and  $Re_{D_h}$  is the Reynolds number based on the hydraulic diameter  $D_h$ . Thus, Karamanis & Hodes (2019a) provide  $\overline{Nu}$  as a function of  $\varepsilon$ , t,  $k/k_f$ ,  $L^+$ ,  $Re_{D_h}$  and Pr (the Prandtl number). Finally, Karamanis & Hodes (2019b) combined the results for Po and  $\overline{Nu}$  from the foregoing studies with flow network modelling and multi-variable optimisation to find the optimal fin thickness, spacing, height and length for an array of heat sinks in a circuit pack such as a blade server, laptop or rack-mountable electronics or optoelectronics. Since then, there have been other numerical studies reporting optimal heat sink geometries. Representatively, Martin et al. (2022) and Sun, Ismail & Mustaffa (2025) optimised the aspect ratio of the ducts by a brute-force numerical method over a limited parameter space, with Sun et al. (2025) employing machine learning optimisation techniques.

More recently, the hydrodynamic problem with (c>0) or without clearance (c=0) was revisited by Miyoshi *et al.* (2024). They considered the limit of small fin spacing  $\varepsilon \ll 1$ , which is typical in practice – see table 1. For example, Iyengar & Bar-Cohen (2007) report the minimum values to range from 1/60 (bonding) up to 1/6 (die casting), or approximately  $\varepsilon \approx 0.015-0.15$ . Although no clearance is ideal (c=0), finite clearance (c>0) is common, with the range of c being highly variable. It may be as low as,

Parameter	Values	Range
ε	1/60 (bonding), 1/50 (forging, machining),	≈0.015-0.15
	1/25 (skiving), 1/8 (extruding)	
С	0 (fully shrouded), 0.01 (allowing for thermal expansion),	(highly variable)
	$\gtrsim 1$ (for low-power components)	
$\Omega$	1.6–11.7 (Copper–water), 22–150 (Aluminium–air)	$\approx 1-150$
Re	400–2600 (water, microchannel heat sink), >5000 (air)	(highly variable)

Table 1. Typical parameter values possible in practical LFHSs. The  $\varepsilon$  values are the minimum for different manufacturing methods as reported by Iyengar & Bar–Cohen (2007). We also used corresponding fin thicknesses ( $t^*$ ) therein to estimate  $\Omega$ . Re ranges from experiments Reyes et al. (2011) (water), Sparrow & Kadle (1986) (air).

say, 0.01, when a small gap is left between fin tips and an adjacent circuit board to accommodate thermal expansion. On the other hand, for lower power components, flow bypass is common and the clearance may exceed the fin height (c > 1). In the small  $\varepsilon$  limit, Miyoshi *et al.* (2024) presented new flow solutions and Po formulas for a range of clearances, using complex conformal maps and matched asymptotic expansions.

The analysis of Miyoshi *et al.* (2024) was limited to the hydrodynamic problem. In this companion paper we consider the corresponding conjugate thermal problem (i.e. precisely the one numerically solved by Sparrow *et al.* 1978) in the limit of small fin spacing ( $\varepsilon \ll 1$ ) with finite clearance (c > 0). We derive explicit formulas for the coupled temperature fields in the fluid and the fin, and the local and overall heat transfer quantities as a function of  $\varepsilon$ , c and  $\Omega$ , thereby replacing many of the numerical results of Sparrow *et al.* (1978). To validate these formulas, we compare them with our numerical solutions of the full model, as well as the (equivalently) results of Sparrow *et al.* (1978). Two approximations (leading order and higher order, respectively) for the average Nusselt number are found to take the simple forms

$$\overline{Nu}^{(0)} = \frac{2.4304 \,\varepsilon}{c(2+\varepsilon)} + O(\varepsilon^2),\tag{1.2}$$

$$\overline{Nu}^{(1)} = \frac{\varepsilon}{c(2+\varepsilon)} \left[ 2.4304 - \frac{\varepsilon}{c} \left( 0.5362 + \frac{2.6449}{\Omega} \right) \right] + O(\varepsilon^3), \tag{1.3}$$

and their comparisons with numerical solutions are summarised in figures 9, 10 and 11. The numerical constants in the above, shown to 4 decimal places, are readily calculated to arbitrary precision.

We note that, in practice, heat sinks on low-power components in circuit packs, such as voltage regulators, metal–oxide–semiconductor field-effect transistors (MOSFETs) and memory, are not fully shrouded, i.e. c in figure 1 is finite. Minimising the cost, weight, size, etc. of them, albeit a secondary consideration in an overall thermal management solution, requires knowledge of how the conjugate Nusselt numbers depend upon the solid–fluid combination and the geometry of the heat sink via  $\Omega$ ,  $\varepsilon$  and c. Moreover, it further depends upon the corresponding Poiseuille numbers, which in turn, depend upon  $\varepsilon$  and c, as per our companion study (Miyoshi *et al.* 2024). Indeed, the caloric resistance of a heat sink, i.e. that associated with the bulk temperature rise of the fluid, is also important (Karamanis & Hodes 2016). Furthermore, the inlet fluid velocity and temperature profiles to the heat sinks on the high-power components (where c is normally 0), such as central processing units (CPUs), are affected by the pressure drops and temperature rises as fluid flows through the heat sinks on low-power ones.

Another practical consideration is whether or not the flow is hydrodynamically and thermally fully developed as assumed here. The values of  $L^+$  corresponding to hydrodynamically fully developed flow in rectangular ducts (c = 0) are well known, as per the aforementioned study by Curr et al. (1972). Moreover, since the Prandtl numbers for air and water are approximately 0.7 and 7, respectively, when the flow is hydrodynamically fully developed, it may be assumed to be thermally fully developed. However, to our knowledge, development lengths for the problem when c > 0 have not been considered and is beyond the scope of the present study. In the case of c = 0, it is very common for hydrodynamically and thermally fully developed flow to be a valid assumption as per, e.g. in the direct liquid cooling of a CPU (Zhang et al. 2015). Further, the Reynolds number Re (based on the hydraulic diameter) is commonly low enough for laminar flow, e.g. in the range 400-2600 in water microchannel heat sinks (Reyes et al. 2011), but it can also be transitional or turbulent for air (Sparrow & Kadle 1986). Nonetheless, for fully developed laminar flow (which we provide formulas for in this paper), the conclusions of Sparrow et al. (1978), that tip clearance results in a significant reduction in heat transfer, have been qualitatively borne out by experimental works in subsequent decades (Reves et al. 2011).

The paper is structured as follows. The mathematical problem is formulated in § 2. A summary of the solutions to the flow and thermal problems in the narrow-fin-spacing limit ( $\varepsilon \ll 1$ ) is presented in § 3. The Nusselt number definitions and formulas are given in § 4, and they are compared with numerical solutions in § 5, followed by conclusions in § 6.

#### 2. Problem formulation

In this section we formulate the problem as given in Sparrow *et al.* (1978). A schematic of the shrouded heat sink is shown in figure 1, including all dimensional lengths (and their non-dimensional ratios). The fin array is periodic and aligned longitudinally with the flow direction. The fin thickness is assumed to be negligible compared with other lengths, except for the purpose of heat conduction along it. Throughout, an asterisk will denote that a variable or length is dimensional (thermophysical properties are always dimensional). We assume that the flow is hydrodynamically and thermally fully developed, and consider the coupled (conjugate) thermal problems in the fluid and fins simultaneously.

The flow is unidirectional in the  $z^*$  direction. The velocity field,  $w^*(x^*, y^*)$ , is governed by

$$\frac{\partial^2 w^*}{\partial x^{*2}} + \frac{\partial^2 w^*}{\partial y^{*2}} = \frac{1}{\mu} \frac{\mathrm{d}p^*}{\mathrm{d}z^*} \quad \text{in } \mathcal{D}, \tag{2.1}$$

where  $\mu$  is the dynamic viscosity and  $\mathrm{d}p^*/\mathrm{d}z^*$  is the constant pressure gradient. By periodicity, we restrict attention to a single fin period,  $\mathcal{D} = \{0 \le x^* \le S^*, 0 \le y^* \le H^* + C^*\}$ . The flow satisfies no slip  $(w^* = 0)$  on the fin  $(x^* = 0)$  and  $0 < y^* < H^*$ , base  $(y^* = 0)$  and shroud  $(y^* = H^*)$ , and symmetry  $(\partial w^*/\partial x^* = 0)$  along the centreline between adjacent fins  $(x^* = S^*/2)$  and above each fin  $(x^* = 0)$  and  $(y^* = 0)$  and  $(y^* = 0)$  and  $(y^* = 0)$  and  $(y^* = 0)$  and above each fin  $(y^* = 0)$  and  $(y^* =$ 

The thermal energy equation in the fluid takes the form

$$w^* \frac{\partial T^*}{\partial z^*} = \alpha \left( \frac{\partial^2 T^*}{\partial x^{*2}} + \frac{\partial^2 T^*}{\partial y^{*2}} \right) \quad \text{in } \mathcal{D}, \tag{2.2}$$

where  $T^*(x^*, y^*, z^*)$  is the fluid temperature and  $\alpha$  is its thermal diffusivity. We assume that the base is isothermal, at temperature  $T^*_{base}$ ; hence, the fully developed assumption

implies

$$\frac{\partial T^*}{\partial z^*} = \frac{T^*(x^*, y^*, z^*) - T^*_{base}}{T^*_b(z^*) - T^*_{base}} \frac{\mathrm{d}T^*_b}{\mathrm{d}z^*},\tag{2.3}$$

where

$$T_b^* = \frac{\int_{\mathcal{D}} w^* T^* \, \mathrm{d}A^*}{\int_{\mathcal{D}} w^* \, \mathrm{d}A^*},\tag{2.4}$$

is the bulk fluid temperature. Boundary conditions specifying an isothermal base, adiabatic shroud, and symmetry above the fins  $(x^* = 0)$  and between them  $(x^* = S^*/2)$  are given by

$$T^* = T_{base}^*$$
 on  $y^* = 0$ , (2.5)

$$T^* = T_{base}^* \qquad \text{on } y^* = 0, \tag{2.5}$$

$$\frac{\partial T^*}{\partial y^*} = 0 \qquad \text{on } y^* = H^* + C^*, \tag{2.6}$$

$$\frac{\partial T^*}{\partial x^*} = 0 \qquad \text{on } x^* = 0, \quad H^* < y^* < H^* + C^*, \tag{2.7}$$

$$\frac{\partial T^*}{\partial x^*} = 0 \qquad \text{on } x^* = S^*/2, \quad 0 < y^* < H^* + C^*, \tag{2.8}$$

$$\frac{\partial T^*}{\partial x^*} = 0$$
 on  $x^* = 0$ ,  $H^* < y^* < H^* + C^*$ , (2.7)

$$\frac{\partial T^*}{\partial x^*} = 0$$
 on  $x^* = S^*/2$ ,  $0 < y^* < H^* + C^*$ , (2.8)

respectively. On the fin surface, we have continuity of temperature and heat flux with the conduction problem within the fin. The Biot number based on fin thickness is assumed to be small enough that the temperature across its width is approximately constant, with significant temperature variations occurring only along its height. Performing an energy balance across half the width,  $t^*$ , of the fin (only half is relevant to the domain considered), conduction up the fin is governed by the one-dimensional equation

$$\frac{k_f t^*}{2} \frac{d^2 T_f^*}{dy^{*2}} = -k \left. \frac{\partial T^*}{\partial x^*} \right|_{x^* = 0}, \quad \text{for } 0 < y^* < H^*,$$
 (2.9)

where  $T_f^*$  is the fin temperature. The sink term on the right-hand side corresponds to heat conducting (at each  $y^*$  location) out of the fin and into the fluid. We remark that the 'small Biot number' assumption can be translated explicitly into an assumption on the conductivity ratio  $k_f/k$ . Typically  $k_f/k$  will be large (e.g.  $O(10^4)$  for aluminium and air) and, mathematically, to allow conduction up the fin when taking the limit of small thickness  $(t^*/H^* \ll 1)$  we must have  $k_f/k = O((t^*/H^*)^{-1})$  or larger. (This can be shown rigorously by considering the limit  $t^*/H^* \rightarrow 0$  of the two-dimensional conduction problem in the fin, while taking the distinguished limit  $k_f/k = O((t^*/H^*)^{-1})$  so that the product  $k_f t^*/(2kH^*) = \Omega$  stays fixed) Or in terms of  $\Omega$  (given by (1.1)), this is equivalent to  $\Omega = O(1)$  or larger. This assumption allows the temperature variations up the fin to be comparable to the temperature variations in the fluid.

There is also temperature continuity between the fin and fluid

$$T_f^* = T^* \big|_{x^* = 0}, \quad \text{for } 0 < y^* < H^*.$$
 (2.10)

(Note, axial conduction in  $z^*$  in the fin is also neglected for fully developed flow, as is typical for axially constant temperature boundary conditions – see (Shah & London 1978, Chapter 2) – because the ratio of axial conduction to transverse conduction scales the same way in both the fin and fluid, and so both are negligible if the axial Péclet number is large). Of course, there is another identical fin at  $x^* = S^*$  with the same temperature  $T_f^*$ , but in practice we enforce symmetry down the centreline at  $x^* = S^*/2$  instead.

Finally, the isothermal condition at the base and adiabatic condition at the tip (due to its negligible surface area) are, respectively,

$$T_f^* = T_{base}^*, \quad \text{at } y^* = 0,$$
 (2.11)

$$T_f^* = T_{base}^*, \quad \text{at } y^* = 0,$$
 (2.11)  
 $\frac{dT_f^*}{dv^*} = 0, \quad \text{at } y^* = H^*.$  (2.12)

#### 2.1. Non-dimensional equations

The flow problem (2.1) is non-dimensionalised by scaling  $x^*$  and  $y^*$  with  $H^*$  and the velocity with  $(-\partial p^*/\partial z^*)H^{*2}/\mu$ , i.e. introducing

$$x = x^*/H^*,$$
  $y = y^*/H^*,$   $w = \frac{\mu}{(-dp^*/dz^*)H^{*2}}w^*,$  (2.13)

resulting in a non-dimensional streamwise momentum (Poisson) equation of the form

$$\frac{\partial^2 w}{\partial x^2} + \frac{\partial^2 w}{\partial y^2} = -1 \quad \text{in } \mathcal{D}. \tag{2.14}$$

It is subjected to the boundary conditions

$$w = 0$$
 on  $y = 0, 1 + c,$  (2.15)

$$w = 0$$
 on  $y = 0$ ,  $1 + c$ , (2.15)  
 $w = 0$  on  $x = 0$ ,  $\varepsilon$ ,  $0 < y < 1$ , (2.16)

$$\frac{\partial w}{\partial x} = 0$$
 on  $x = 0$ ,  $\varepsilon$ ,  $1 < y < 1 + c$ , (2.17)

where the non-dimensional geometric parameters are then  $\varepsilon = S^*/H^*$ , the ratio of fin spacing to fin height, and  $c = C^*/H^*$ , the ratio of clearance to fin height.

As in Sparrow et al. (1978), we define a non-dimensional temperature field in the fluid as

$$T = \frac{T^* - T_{base}^*}{T_b^* - T_{base}^*},\tag{2.18}$$

and a non-dimensional streamwise coordinate as

$$z = \frac{\alpha z^*}{\overline{w^*} H^{*2}},\tag{2.19}$$

where  $\overline{w}^*$  is the average velocity

$$\overline{w}^* = \frac{1}{S^*(H^* + C^*)} \int_{\mathcal{D}} w^* dA^*.$$
 (2.20)

Expressing (2.2) in non-dimensional form, we have

$$\lambda WT = \frac{\partial^2 T}{\partial x^2} + \frac{\partial^2 T}{\partial y^2} \quad \text{in } \mathcal{D}, \tag{2.21}$$

where we have defined  $W = w/\overline{w}$ , and

$$\lambda = \frac{1}{T_b^* - T_{base}^*} \frac{dT_b^*}{dz},$$
 (2.22)

is the non-dimensional exponential decay rate of  $T_b^* - T_{base}^*$ , which is a negative constant due to the fully developed assumption. This constant is fixed by enforcing the definition of the bulk temperature, which in non-dimensional terms must be equal to one, i.e.

$$\frac{1}{\varepsilon(1+c)} \int_{\mathcal{D}} WT \, dA = 1. \tag{2.23}$$

The corresponding boundary conditions (2.5)–(2.8) become

$$T = 0$$
 on  $y = 0$ , (2.24)

$$T = 0$$
 on  $y = 0$ , (2.24)  
 $\frac{\partial T}{\partial y} = 0$  on  $y = 1 + c$ , (2.25)

$$\frac{\partial T}{\partial x} = 0 \qquad \text{on } x = 0, \quad 1 < y < 1 + c, \tag{2.26}$$

$$\frac{\partial T}{\partial x} = 0$$
 on  $x = \varepsilon/2$ ,  $0 < y < 1 + c$ . (2.27)

Defining the non-dimensional fin temperature  $T_f$  as in (2.18), where T and  $T^*$  are replaced by  $T_f$  and  $T_f^*$ , the thermal problem in the fin, (2.9)–(2.12), becomes

$$\Omega \frac{\mathrm{d}^2 T_f}{\mathrm{d}y^2} = -\left. \frac{\partial T}{\partial x} \right|_{x=0}, \quad \text{for } 0 < y < 1, \tag{2.28}$$

$$T_f = T|_{x=0}$$
, for  $0 < y < 1$ , (2.29)

$$T_f = 0$$
, at  $y = 0$ , (2.30)

$$\frac{\mathrm{d}T_f}{\mathrm{d}y} = 0, \quad \text{at } y = 1, \tag{2.31}$$

where  $\Omega$  (given by 1.1) is the product of the fin-to-fluid conductivity ratio and the fin's (small) thickness-to-height ratio. The limit  $\Omega \to \infty$  corresponds to an isothermal fin, where T = 0 along the entire fin surface.

The above non-dimensional system of equations can be solved in their current form, but for consistency with the literature and to yield a more convenient equation for  $\lambda$ , we instead solve for the scaled temperatures

$$\phi = \frac{T}{\lambda}, \qquad \qquad \phi_f = \frac{T_f}{\lambda}. \tag{2.32}$$

Under this transformation, all equations and boundary conditions remain unchanged (T and  $T_f$  replaced with  $\phi$  and  $\phi_f$ , respectively), except for the integral condition (2.23) which becomes

$$\lambda = \frac{\varepsilon(1+c)}{\int_{\mathcal{D}} \mathcal{W}\phi \, dA},\tag{2.33}$$

with  $\lambda$  now appearing explicitly.

#### 3. Solutions in the small-fin-spacing limit

We consider the flow and conjugate thermal problems, i.e. (2.14)-(2.17) and (2.21)-(2.33), respectively, in the geometric limit where the fin spacing is small in comparison with the fin height, i.e.  $\varepsilon = S^*/H^* \ll 1$ . This is typical of real heat sinks by design, to increase the total surface area for heat transfer; see table 1 and, e.g. the photographs of heat sinks used

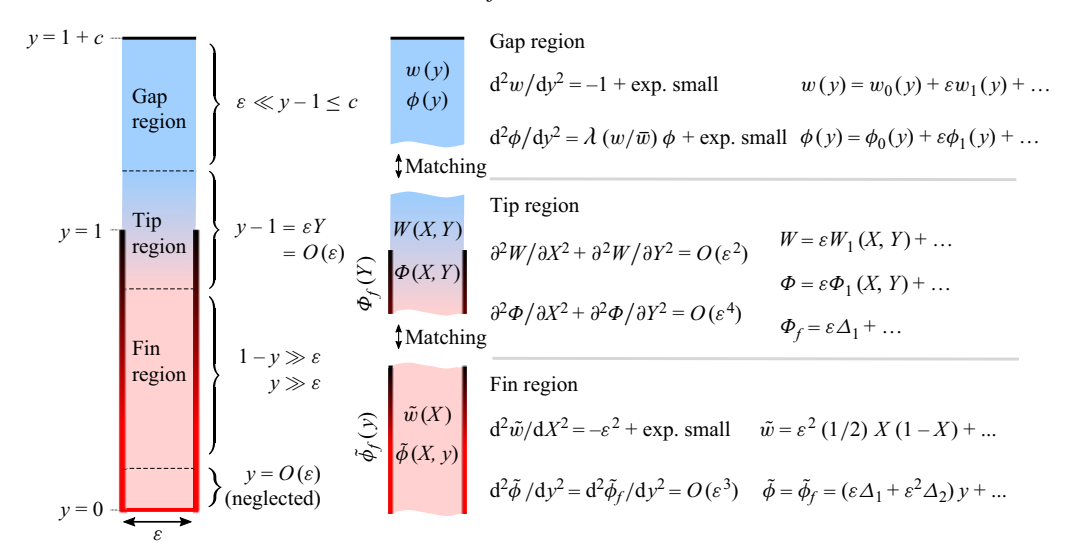


Figure 2. Asymptotic structure of the domain showing the gap, tip and fin regions, and the behaviour of the velocity and temperature expansions in each region (the region close to the base,  $y = O(\varepsilon)$ , is not considered here).

in the thermal management of electronics in Iyengar & Bar-Cohen (2007). Importantly, we will further assume that the non-dimensional tip clearance,  $c = C^*/H^*$ , will remain of order 1 as we take  $\varepsilon \to 0$ . This is common for lower-power components on a printed wiring board (say, voltage regulators) which use smaller heat sinks than higher-power ones (say, a central processing unit). The hydrodynamic problem in this limit has already been considered by Miyoshi et al. (2024), and we present here corresponding solutions for the thermal problem. It is instructive to summarise the hydrodynamic solution first, before presenting a summary of the temperature solution. The full derivation of the temperature solution can be found in Appendix A.

#### 3.1. Summary of hydrodynamic solution

It is convenient to rescale the x coordinate by defining  $X = x/\varepsilon$ , so that the problem domain is independent of  $\varepsilon$ . Then, (2.14)–(2.17) become

$$\frac{1}{\varepsilon^2} \frac{\partial^2 w}{\partial X^2} + \frac{\partial^2 w}{\partial y^2} = -1 \quad \text{in } \mathcal{D} = \{0 < X < 1, \ 0 < y < 1 + c\},\tag{3.1}$$

$$w = 0$$
 on  $y = 0, 1 + c,$  (3.2)

$$w = 0$$
 on  $X = 0, 1, 0 < y < 1,$  (3.3)

$$w = 0$$
 on  $y = 0$ ,  $1 + c$ , (3.2)  
 $w = 0$  on  $X = 0$ ,  $1$ ,  $0 < y < 1$ , (3.3)  
 $\frac{\partial w}{\partial X} = 0$  on  $X = 0$ ,  $1$ ,  $1 < y < 1 + c$ . (3.4)

Considering now  $\varepsilon \to 0$ , the asymptotic solution takes a different form depending on the region in the domain. Employing matched asymptotic expansions, the domain decomposes into a gap region (1 < y < 1 + c) above the fins, a fin region (0 < y < 1) between the fins (but at least a distance  $O(\varepsilon)$  away from their base or tips) and a short tip region near the fin tips  $(y-1=O(\varepsilon))$  that transitions between them. There is also a small base region,  $(y = O(\varepsilon))$  but it is not relevant to the thermal analysis (see Miyoshi et al. 2024 for more details). A schematic of the different regions and the resulting problems within each, is shown in figure 2.

### 3.1.1. *Gap region:* $1 < y \le 1 + c$

In the gap region above the fins, a regular expansion  $w = w_0 + \varepsilon w_1 + \cdots$  for  $\varepsilon \ll 1$  leads to the result that w is independent of X (i.e. only a function of y) to all algebraic orders. Thus the unit pressure gradient, and the no-slip condition on the shroud (y = 1 + c) lead to a Poiseuille-type parabolic flow profile. The leading-order flow is

$$w_0(y) = -\frac{1}{2}(y-1)(y-1-c), \tag{3.5}$$

and the  $O(\varepsilon)$  correction is a shear flow

$$w_1(y) = -\frac{\log 2}{2\pi}(y - 1 - c), \tag{3.6}$$

that is induced by the non-parabolic flow in the tip region, which is discussed after we present the solution in the fin region.

# 3.1.2. *Fin region:* 0 < y < 1

Denoting the solution in this region by  $\tilde{w}$ , a regular expansion  $\tilde{w} = \tilde{w}_0 + \varepsilon \tilde{w}_1 + \cdots$  leads this time to a Poiseuille flow but with variation in the X direction. This is because the flow must satisfy no-slip conditions on the fins at X = 0 and 1. The result is that

$$\tilde{w} = \frac{1}{2}\varepsilon^2 X(1-X) + \cdots, \tag{3.7}$$

where any higher orders are beyond all algebraic powers, and thus are exponentially small in  $\varepsilon$ .

Interestingly, the flow in both the gap and fin regions is parabolic, but with variations oriented perpendicularly to one another. The transition between the two solutions takes place in the tip region, where the solution varies in both the X and y directions.

The no-slip condition at the bottom of the domain, y = 0, can be easily satisfied by the inclusion of a simple series, which is exponentially small unless  $y = O(\varepsilon)$ , i.e. close to the domain bottom. The modified solution is (Miyoshi *et al.* 2024)

$$\tilde{w}(X, y) = \frac{1}{2} \varepsilon^2 X (1 - X) - 4\varepsilon^2 \sum_{n = 1, 3, \dots} \frac{e^{-n\pi y/\varepsilon} \sin n\pi X}{n^3 \pi^3}.$$
 (3.8)

This is typically only relevant for visualising the flow field, since the effect of the base region on the average velocity is negligible.

#### 3.1.3. Tip region: $y - 1 = O(\varepsilon)$

Near the fin tips, i.e. an  $O(\varepsilon)$  distance away, the variation in X becomes important; therefore, we introduce the inner variable  $Y = (y - 1)/\varepsilon$  which is O(1) in this region, and we denote the solution here by w = W(X, Y).

It turns out that asymptotic matching with the gap region above  $(Y \to +\infty)$  implies that the solution is  $O(\varepsilon)$  here at leading order

$$W = \varepsilon W_1(X, Y) + O(\varepsilon^2), \tag{3.9}$$

and  $W_1(X,Y)$  (from (3.1), (3.3) and (3.4)) satisfies in the infinite strip  $\mathcal{D}_{tip} =$  $\{0 < X < 1, -\infty < Y < \infty\}$ 

$$\nabla_{XY}^2 W_1 = 0 \qquad \text{in } \mathcal{D}_{tip}, \tag{3.10}$$

$$W_1 = 0$$
 on  $X = 0, 1, Y < 0,$  (3.11)

$$\nabla_{XY}^{2} W_{1} = 0 \quad \text{in } \mathcal{D}_{tip},$$

$$W_{1} = 0 \quad \text{on } X = 0, 1, \quad Y < 0,$$

$$\frac{\partial W_{1}}{\partial X} = 0 \quad \text{on } X = 0, 1, \quad 0 < Y,$$
(3.10)
$$(3.11)$$

where  $\nabla_{XY}^2 = \partial^2/\partial X^2 + \partial^2/\partial Y^2$ , and the asymptotic matching conditions

$$W_1 \sim \frac{1}{2}cY$$
 as  $Y \to \infty$ , (3.13)

$$W_1 \to 0$$
 as  $Y \to -\infty$ . (3.14)

This has the convenient solution in terms of a complex variable (Miyoshi et al. 2024)

$$W_1 = -\frac{c}{2\pi} \log \left| \frac{e^{i\pi/4} - \tan^{1/2}(\pi Z/2)}{e^{i\pi/4} + \tan^{1/2}(\pi Z/2)} \right|, \quad \text{where } Z = X + iY.$$
 (3.15)

Notably, a constant term  $c \log 2/(2\pi)$  that perturbs the shear term Y in the limit  $Y \to \infty$ follows from this solution, since

$$W_1 \sim \frac{1}{2}c \left[ Y + \frac{\log 2}{\pi} + O(e^{-\pi Y}) \right] \quad \text{as } Y \to \infty, \tag{3.16}$$

and matching at  $O(\varepsilon)$  with the gap region solution leads to the response  $w_1$ , given by (3.6).

# 3.1.4. *Composite flow solutions*

A pair of composite flow solutions valid through larger regions of the domain can be constructed by adding solutions in adjacent regions and subtracting the solution in the overlap region between them. When patched together in a piece-wise fashion, these can be used to construct a single global flow field if desired. We do so by splitting the domain into  $y \ge 1$  and y < 1 (i.e. at the fin tips), and then constructing a composite solution in each region separately.

A gap-tip composite (restricted to  $1 \le y \le 1 + c$ ) is given by

$$w_{gap-tip} = \underbrace{w_0(y) + \varepsilon w_1(y)}_{\text{gap region}} + \underbrace{\varepsilon W_1\left(X, \frac{y-1}{\varepsilon}\right)}_{\text{tip region}} - \underbrace{\frac{c}{2}\left(y-1+\frac{\varepsilon \log 2}{\pi}\right)}_{\text{gap-tip overlap}},$$

$$= -\frac{1}{2}(y-1-c)\left(y-1+\frac{\varepsilon \log 2}{\pi}\right) + \varepsilon W_1\left(X, \frac{y-1}{\varepsilon}\right), \qquad 0 < X < 1.$$
(3.17)

On the other hand, a one-term composite (say restricted to  $0 \le y < 1$ ) between the tip and fin regions is given simply by the tip solution  $\varepsilon W_1$ , since it matches with 'zero' appearing at that order in the fin region. Strictly, to bring in the  $O(\varepsilon^2)$  parabolic flow from the fin region one would require a two-term composite, but we do not possess a second term (of  $O(\varepsilon^2)$ ) in the tip region. However, we can form an *ad hoc* composite with an  $O(\varepsilon^2)$  error in the tip region, by simply superimposing the tip and fin region solutions

$$w_{tip\text{-}fin} = \underbrace{\varepsilon W_1\left(X, \frac{y-1}{\varepsilon}\right)}_{\text{tip region}} + \underbrace{\tilde{w}(X, y)}_{\text{fin region}}, \qquad 0 < X < 1. \tag{3.18}$$

#### T.L. Kirk and M. Hodes

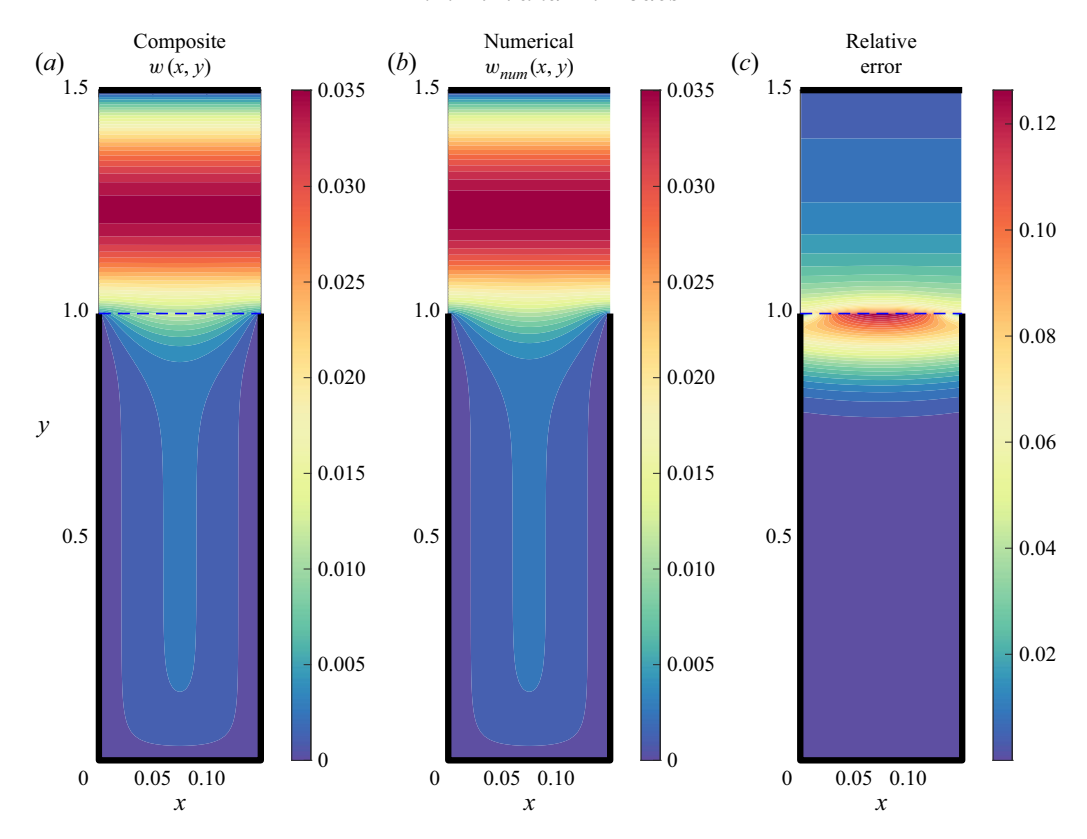


Figure 3. The asymptotic piece-wise composite solution (3.17)–(3.18) for the velocity field w(x, y) in one period (a), compared with the numerical velocity  $w_{num}$  (b), with the local relative error  $|w(x, y) - w_{num}(x, y)|/|w_{num}|$  (c). Geometric parameters are  $\varepsilon = 0.15$  and c = 0.5. The asymptotic solution consists of two composites: one valid for  $y \ge 1$ , and one for y < 1, and the separating line (y = 1) is shown as a dashed blue line. The fins (at  $0 \le y \le 1$ , x = 0, 1) and base are shown in black.

This is used here purely to allow visualisation of the flow field in figures (i.e. Figure 3), and not for further detailed calculations. Here,  $W_1(X, Y)$  is (3.15) and  $\tilde{w}(X, y)$  is (3.8). Even though it has an  $O(\varepsilon^2)$  error in the tip region, the correct leading-order behaviour is exhibited in each of the (tip and fin) regions, and so the main flow features are retained.

#### 3.1.5. Poiseuille number

The mean velocity is given by

$$\overline{w} = \frac{1}{1+c} \int_0^1 \int_0^{1+c} w \, dy dX = \frac{c^3}{12(1+c)} \left[ 1 + \frac{\varepsilon \log 8}{\pi c} \right] + O(\varepsilon^2), \tag{3.19}$$

where the contributions from the tip region (velocity of  $O(\varepsilon)$  over a region of area  $O(\varepsilon)$ ) and fin region (velocity of  $O(\varepsilon^2)$  over a region of area O(1)) are both  $O(\varepsilon^2)$ , so  $\overline{w}$  up to  $O(\varepsilon)$  follows only from the gap solution (3.5), (3.6).

The friction factor is defined as (Sparrow *et al.* 1978)

$$f = \frac{(-\mathrm{d}p^*/\mathrm{d}z^*)D_e^*}{\frac{1}{2}\rho\overline{w}^{*2}}, \qquad D_e^* = \frac{4(H^* + C^*)S^*}{2(H^* + S^*)}, \qquad (3.20)$$

and the Poiseuille number is then Po = fRe where  $Re = \rho \overline{w}^* D_e^* / \mu$  is the Reynolds number and  $\rho$  is the fluid density. In terms of non-dimensional quantities,

$$Po = fRe = \frac{8(1+c)^2 \varepsilon^2}{\overline{w}(1+\varepsilon)^2}.$$
 (3.21)

Substituting the asymptotic solution (3.19) for  $\overline{w}$  results in the elementary expression (Miyoshi *et al.* 2024)

$$Po = \frac{96(1+c)^3 \varepsilon^2}{c^2 \left(c + \frac{\varepsilon \log 8}{\pi}\right) (1+\varepsilon)^2} + O(\varepsilon^4), \quad \text{as } \varepsilon \to 0.$$
 (3.22)

This expression was compared with an exact solution valid for arbitrary  $\varepsilon$  in Miyoshi et al. (2024), and shown to be accurate to within 15% if  $\varepsilon \lesssim 0.3c$ . As expected, the approximation breaks down when c becomes small (i.e. comparable to  $\varepsilon$ ). Thus, for a given accuracy, the range of  $\varepsilon$  must shrink to maintain validity.

# 3.2. Summary of temperature solution

Here, we provide a summary of the temperature solution in the limit  $\varepsilon \to 0$ , which has a similar asymptotic domain decomposition as for the hydrodynamic problem – see figure 2 for a schematic summary of the domain regions. Indeed, the hydrodynamic solution plays an important role in the temperature one. It is important to note here at the outset that  $\lambda$ , the constant given by the integral formula (2.33), will be mostly determined by the behaviour in the gap region above the fins since the flow there dominates the integral. This leads to  $\lambda = O(1)$ , and  $\phi = O(1)$  in the gap. A full derivation of the following solution is given in Appendix A.

# 3.2.1. *Fin region* $(0 \le y < 1, 1 - y \gg \varepsilon)$

In the fin region, since the flow is relatively small, i.e.  $\mathcal{W} = w/\overline{w} = O(\varepsilon^2)$  compared with O(1) in the gap region (1 < y < 1 + c), advection is negligible and therefore the heat transfer is purely conductive (until  $O(\varepsilon^3)$ ). Furthermore, the narrow fin spacing leads to the temperature here (denoted by  $\tilde{\phi}$  in the fluid, and  $\phi_f$  in the fin), to be uniform in X and only depend on y. It varies linearly in y since the conduction is one dimensional and predominantly due to conduction up the fins. The solution (to the first two orders in  $\varepsilon$ ) is

$$\phi_f = \tilde{\phi} = \varepsilon \tilde{\phi}_1(y) + \varepsilon^2 \tilde{\phi}_2(y) + O(\varepsilon^3) = -(1+c) \left( \frac{\varepsilon}{2\Omega} - \frac{\varepsilon^2}{4\Omega^2} \right) y + O(\varepsilon^3). \quad (3.23)$$

In the case where the fins have infinite conductivity  $\Omega=\infty$  (i.e. are isothermal), then  $\tilde{\phi}\equiv\phi_f=0$  to the order considered.

### 3.2.2. *Tip region* $(y - 1 = \varepsilon Y, Y = O(1))$

Here, close to the fin tips, the temperature field (denoted by  $\Phi(X,Y)$  in the fluid and  $\Phi_f(Y)$  in the fin) becomes two-dimensional but the heat transfer is still purely conductive since advection is still negligible. This is because the flow field here has  $\mathcal{W} = w/\overline{w} = O(\varepsilon)$ , leading to advective terms being three orders higher than the diffusive terms, which dominate. To the order considered, the entirety of the heat transfer from the fin to fluid occurs here in the tip region.

The temperature in the fin near the tip is simply constant at leading order

$$\Phi_f = \varepsilon \Phi_{f1} + O(\varepsilon^2) = -\frac{\varepsilon(1+c)}{2\Omega} + O(\varepsilon^2), \tag{3.24}$$

and the  $O(\varepsilon^2)$  correction is given by the simple integral (C14). The temperature in the fluid at leading order

$$\Phi = \varepsilon \Phi_1(X, Y) + O(\varepsilon^2) \quad \text{in } \mathcal{D}_{tip} = \{0 < X < 1, -\infty < Y < \infty\}, \tag{3.25}$$

is governed by the same problem as the velocity field  $W_1(X, Y)$  (up to an additive constant and scaling factor) and hence, conveniently, the same complex variable solution can be employed again, giving

$$\Phi_1 = -\frac{1+c}{2\Omega} - \frac{2(1+c)}{c} W_1(X,Y), \tag{3.26}$$

where  $W_1$  is (3.15). The far-field behaviours (matching with the gap region above, and fin region below) are

$$\Phi_1 \sim -(1+c) \left[ Y + \frac{\log 2}{\pi} + \frac{1}{2\Omega} + O(e^{-2\pi Y}) \right] \quad \text{as } Y \to \infty,$$
(3.27)

$$\Phi_1 \to -\frac{1+c}{2\Omega} \quad \text{as } Y \to -\infty.$$
(3.28)

# 3.2.3. *Gap region* $(1 < y \le 1 + c, y - 1 \gg \varepsilon)$

Finally, in this region above the fins, advection is now important and balances conduction. Further, the problem depends only on y to all orders in  $\varepsilon$ , e.g.  $\phi = \phi_0(y) + \varepsilon \phi_1(y) + \varepsilon \phi_1(y)$  $O(\varepsilon^2)$  (just as for the velocity field) and the constant  $\lambda$ , with expansion  $\lambda = \lambda_0 + \varepsilon \lambda_1 + \varepsilon \lambda$  $O(\varepsilon^2)$ , is now relevant and can be determined. The leading-order problem for  $(\phi_0, \lambda_0)$  is the classical problem with an isothermal, no-slip 'lower boundary' (which here is at y = 1) and an adiabatic, no-slip upper wall at y = 1 + c. The equations ((A14)–(A16) and (A40)) can be transformed to the usual scaling, independent of the gap thickness (clearance c), if we define

$$\hat{y} = (y - 1)/c,$$
  $\widehat{W}_0(\hat{y}) = W_0(y)c/(1 + c),$  (3.29)

$$\hat{\phi}_0 = \phi_0/[c(1+c)],$$
  $\hat{\lambda}_0 = c(1+c)\lambda_0,$  (3.30)

resulting in the problem

$$\hat{\lambda}_0 \widehat{\mathcal{W}}_0(\hat{y}) \hat{\phi}_0 = \frac{\mathrm{d}^2 \hat{\phi}_0}{\mathrm{d}\hat{y}^2} \quad \text{in } 0 < \hat{y} < 1, \tag{3.31}$$

$$\frac{\mathrm{d}\hat{\phi}_0}{\mathrm{d}\hat{y}} = 0 \qquad \text{on } \hat{y} = 1, \tag{3.32}$$

$$\phi_0 = 0$$
 on  $\hat{y} = 0$ , (3.33)

$$\hat{\phi}_{0} = 0 \quad \text{on } \hat{y} = 0,$$

$$\hat{\lambda}_{0} = \frac{1}{\int_{0}^{1} \widehat{\mathcal{W}}_{0}(\hat{y}) \hat{\phi}_{0}(\hat{y}) \, d\hat{y}},$$
(3.33)

with normalised velocity  $\widehat{\mathcal{W}}_0(\hat{y}) = 6\hat{y}(1-\hat{y})$ . This problem for  $(\hat{\phi}_0, \hat{\lambda}_0)$  has no parameters and is easily solved numerically. We do so using Chebyshev collocation methods to discretise space (Trefethen 2000) and employing an iterative procedure similar to that of (Sparrow *et al.* 1978; Karamanis & Hodes 2016) (and a simpler version of that discussed in § 5.1). We compute the value of  $\hat{\lambda}_0$  (to 4 decimal places)

$$\hat{\lambda}_0 \approx -2.4304. \tag{3.35}$$

The first-order problem for  $(\phi_1, \lambda_1)$  (given by (A17)–(A19) and (A57)) may be transformed in a similar way

$$\hat{y} = (y - 1)/c,$$
  $\widehat{W}_1(\hat{y}) = W_1(y)c^2/(1 + c),$  (3.36)

$$\hat{\phi}_1 = \phi_1/(1+c),$$
  $\hat{\lambda}_1 = c^2(1+c)\lambda_1,$  (3.37)

resulting in

$$(\hat{\lambda}_1 \widehat{\mathcal{W}}_0 + \hat{\lambda}_0 \widehat{\mathcal{W}}_1) \hat{\phi}_0 + \hat{\lambda}_0 \widehat{\mathcal{W}}_0 \hat{\phi}_1 = \frac{d^2 \hat{\phi}_1}{d \hat{y}^2} \quad \text{in } 0 < \hat{y} < 1, \tag{3.38}$$

$$\frac{\mathrm{d}\hat{\phi}_1}{\mathrm{d}\hat{v}} = 0 \qquad \text{on } \hat{y} = 1, \tag{3.39}$$

$$\hat{\phi}_1 = -\left(\frac{\log 2}{\pi} + \frac{1}{2\Omega}\right)$$
 on  $\hat{y} = 0$ , (3.40)

$$\hat{\lambda}_1 = -\hat{\lambda}_0^2 \int_0^1 (\widehat{\mathcal{W}}_0 \hat{\phi}_1 + \widehat{\mathcal{W}}_1 \hat{\phi}_0) \, \mathrm{d}\hat{y}, \tag{3.41}$$

where  $\widehat{\mathcal{W}}_1 = 6(1-\widehat{y})(1-3\widehat{y})\log 2/\pi$ . This problem only depends on the fin conductivity  $\Omega$ , but since it is linear, it can be shown (Appendix D) that the solution takes the form

$$\hat{\lambda}_1 = b_0 + \frac{b_1}{2\Omega},\tag{3.42}$$

where  $b_0$ ,  $b_1$  are numerical constants. Using similar numerical methods to those we employed to find  $\hat{\lambda}_0$ , although even simpler since no iteration is needed, we find that they evaluate to (4 decimal places)

$$b_0 \approx 0.5362,$$
  $b_1 \approx 5.2898.$  (3.43)

Consequently, the solution for  $\lambda$  and its dependence on all the parameters ( $\varepsilon$ , c and  $\Omega$ ) is completely determined. It will be useful to consider two levels of approximation, given by

$$\lambda^{(0)} = \lambda_0 = \frac{\hat{\lambda}_0}{c(1+c)},$$
 (one term) (3.44)

$$\lambda^{(1)} = \lambda_0 + \varepsilon \lambda_1 = \frac{1}{c(1+c)} \left[ \hat{\lambda}_0 + \frac{\varepsilon}{c} \left( b_0 + \frac{b_1}{2\Omega} \right) \right], \quad \text{(two terms)}$$
 (3.45)

where  $\lambda^{(0)}$  is a leading-order approximation (keeping only the  $O(\varepsilon^0)$  term) and  $\lambda^{(1)}$  is a higher-order approximation (keeping terms up to  $O(\varepsilon^1)$ ).

Finally, to transform back to the non-dimensional temperature T anywhere in the domain, you take the product

$$T = \lambda \phi. \tag{3.46}$$

# 3.2.4. Composite temperature field

A composite temperature field, valid throughout the entire domain, can be constructed in the same way as that for the flow field, i.e. by forming composites between adjacent asymptotic regions. Splitting the domain (at the fin tips) into  $y \ge 1$  and y < 1, then we can construct a composite up to  $O(\varepsilon)$  in each subdomain.

A gap–tip composite (restricted to  $1 \le y \le 1 + c$ ) is given by

$$\phi_{gap\text{-}tip} = \underbrace{\phi_0(y) + \varepsilon \phi_1(y)}_{\text{gap region}} + \underbrace{\varepsilon \Phi_1\left(X, \frac{y-1}{\varepsilon}\right)}_{\text{tip region}} - \underbrace{(1+c)\left(-(y-1) - \frac{\varepsilon \log 2}{\pi} - \frac{\varepsilon}{2\Omega}\right)}_{\text{gap-tip overlap}},$$

$$0 < X < 1. \tag{3.47}$$

bearing in mind that the gap solutions  $\phi_0(y)$  and  $\phi_1(y)$  are only known numerically.

A tip–fin composite (restricted to  $0 \le y < 1$ ) between the tip and fin regions up to  $O(\varepsilon)$  is given by

$$\phi_{tip\text{-}fin} = \underbrace{\varepsilon \Phi_1 \left( X, \frac{y-1}{\varepsilon} \right)}_{\text{tip region}} + \underbrace{\varepsilon \tilde{\phi}_1(y)}_{\text{fin region}} + \underbrace{\frac{\varepsilon (1+c)}{2\Omega}}_{\text{overlap}},$$

$$= \varepsilon \Phi_1 \left( X, \frac{y-1}{\varepsilon} \right) - \frac{\varepsilon (1+c)}{2\Omega} (y-1), \qquad 0 < X < 1. \tag{3.48}$$

Also, in the fin itself, a second-order composite solution (for  $0 \le y \le 1$ ) can be found and is given by (C18).

#### 4. Nusselt numbers

In this section we present expressions for various Nusselt numbers as described in Sparrow *et al.* (1978), and approximations for each in the narrow-fin-spacing limit  $\varepsilon \to 0$ .

First, the local Nusselt number on the fin is defined as

$$Nu_f = \frac{q_f^* H^*}{k(T_f^* - T_b^*)} = \frac{1}{1 - \lambda \phi_f} \frac{\lambda}{\varepsilon} \left. \frac{\partial \phi}{\partial X} \right|_{X=0} \quad \text{for } 0 < y < 1.$$
 (4.1)

From the solution in the fin region,  $\partial \phi / \partial X = O(\varepsilon^3)$  at most, hence  $Nu_f$  is only significant close to the fin tips. Substituting the solution there to  $O(\varepsilon)$ , we find,

$$Nu_f(Y) = \lambda_0 \left. \frac{\partial \Phi_1}{\partial X} \right|_{X=0} + O(\varepsilon)$$
 (4.2)

$$= -\frac{\hat{\lambda}_0}{c\sqrt{e^{-2\pi Y} - 1}} + O(\varepsilon), \quad \text{for } Y < 0.$$
 (4.3)

Notice that this leading-order expression does not depend on the fin conductivity  $\Omega$ , and it is singular (with negative square root behaviour) and integrable at the fin tip,  $Y \to 0$ .

Second, the overall heat transfer is captured by the overall Nusselt number

$$\overline{Nu} = \frac{\bar{q}^* H^*}{k(T_{hase}^* - T_h^*)},$$
(4.4)

where 
$$\bar{q}^* = \frac{2\int_0^{H^*} q_f^* dy^* + \int_0^{S^*} q_{base}^* dx^*}{2H^* + S^*},$$
 (4.5)

or in terms of non-dimensional quantities

$$\overline{Nu} = -\lambda \bar{q}, \tag{4.6}$$

where

$$\bar{q} = \frac{1}{2+\varepsilon} \left( 2 \int_0^1 - \frac{\partial \phi}{\partial x} \Big|_{x=0} dy + \int_0^1 - \frac{\partial \phi}{\partial y} \Big|_{y=0} dx \right). \tag{4.7}$$

Here,  $\bar{q}$  is the non-dimensional (with  $\bar{q}^*$  the dimensional) average heat flux, in terms of  $\phi$ , out of the entire heat transfer surface available per period, i.e. two fins (height 1) and the base (width  $\varepsilon$ ). This can be conveniently calculated from the problem statement for  $\phi$ . Integrating (2.21) (with T replaced by  $\phi$ ) over the period domain  $\mathcal{D}$  and applying the divergence theorem

$$\int_{\mathcal{D}} \lambda \mathcal{W} \phi \, dA = 2 \int_{0}^{1} -\left. \frac{\partial \phi}{\partial x} \right|_{x=0} dy + \int_{0}^{1} -\left. \frac{\partial \phi}{\partial y} \right|_{y=0} dx. \tag{4.8}$$

The left-hand side reduces to simply  $\varepsilon(1+c)$  by the definition (2.33) of the constant  $\lambda$ , and the right-hand side equals  $(2+\varepsilon)\bar{q}$ . Hence,  $\bar{q} = \varepsilon(1+c)/(2+\varepsilon)$ , and substituting into (4.6) gives

$$\overline{Nu} = -\lambda \frac{\varepsilon(1+c)}{2+\varepsilon}. (4.9)$$

Substituting the approximation (3.45) for  $\lambda$  in the limit  $\varepsilon \ll 1$  leads to (at least) two levels of approximation for  $\overline{Nu}$ , depending on the number of terms kept

$$\overline{Nu}^{(0)} = -\frac{\varepsilon}{c} \frac{\hat{\lambda}_0}{(2+\varepsilon)} + O(\varepsilon^2), \qquad \text{(leading-order approx)}. \tag{4.10}$$

$$\overline{Nu}^{(1)} = -\frac{\varepsilon}{c} \frac{\left(\hat{\lambda}_0 + \frac{\varepsilon}{c} \hat{\lambda}_1\right)}{2 + \varepsilon} + O(\varepsilon^3), \qquad \text{(higher-order approx)}. \tag{4.11}$$

where  $\overline{Nu}^{(0)}$  is a leading-order approximation (i.e. only the leading term of  $\lambda$  is kept), and  $\overline{Nu}^{(1)}$  a higher-order approximation (where both terms in  $\lambda$  are kept). Note that we do not expand the denominator. We will show later that both of these approximations will have their advantages in practice, even though  $\overline{Nu}^{(1)}$  is strictly of a higher order. Notably, these approximations (4.10)–(4.11) account for heat transfer from both the fin and the base, to the orders considered.

Third, one can define a local Nusselt number on the base as

$$Nu_{base} = \frac{q_{base}^* H^*}{k(T_{base}^* - T_b^*)} = \lambda \left. \frac{\partial \phi}{\partial y} \right|_{y=0} \quad \text{for } 0 < X < 1.$$
 (4.12)

Substituting the solution (3.23) for  $\phi$  in the fin region, and (3.45) for  $\lambda$ , and retaining different orders in  $\varepsilon$  leads to the approximations

$$Nu_{base}^{(0)} = -\frac{\varepsilon \hat{\lambda}_0}{2c\Omega} + O(\varepsilon^2),$$
 (leading-order approx). (4.13)

$$Nu_{base}^{(1)} = -\frac{\varepsilon}{2c\Omega} \left( \hat{\lambda}_0 + \frac{\varepsilon}{c} \hat{\lambda}_1 \right) \left( 1 - \frac{\varepsilon}{2\Omega} \right) + O(\varepsilon^3). \quad \text{(higher-order approx)}. \quad (4.14)$$

#### T.L. Kirk and M. Hodes

This is constant in X to the orders given, and hence the base-averaged Nusselt number  $\overline{Nu}_{base}$  takes the same value.

#### 5. Comparison with numerical solution

To assess the validity of the solutions derived throughout the paper, we compare with numerical solutions of the full hydrodynamic and thermal problems for arbitrary values of the parameters (in particular, arbitrary fin spacing-to-height ratio  $\varepsilon$ ). For a detailed discussion of the impact of  $\varepsilon$  on the general heat transfer behaviour, we refer to Sparrow *et al.* (1978). Here, we focus on the new asymptotic results, and what we can learn from them

# 5.1. Numerical methodology

To solve the full nonlinear two-dimensional problem we employ a domain decomposition and pseudospectral (Chebyshev) collocation methods suited to boundary value problems. The approach is similar to that used by Game *et al.* (2018) and Mayer, Kadoko & Hodes (2021) in a different flow context (superhydrophobic surfaces), and so we give a brief description here with further details given in Supplementary Material.

One half-period is split into 3 subdomains: two fluid (two-dimensional) domains and one fin (one-dimensional) domain, and each are discretised into N+1 points in x (excluding the fin domain) and M+1 points in y using the Gauss-Lobatto spacing for spectral accuracy (Trefethen 2000). This clusters grid points close to domain boundaries (hence even more so for domain corners), and since the fluid domain is subdivided at y=1, many points are clustered close to the singular point ((x,y)=(0,1)) as it sits at the corner of two domains. This helps ensure numerical resolution of the large gradients close to this point where the boundary conditions change type. Continuity of velocity, temperature, shear stress and heat flux were imposed at common boundaries between the fluid subdomains.

The velocity problem discretises into a linear system that is inverted in MATLAB. This is fed into the thermal problem, employing the same mesh (with the addition of the one-dimensional fin domain), which is nonlinear and solved in an iterative fashion. The iteration method is similar to that of Sparrow *et al.* (1978) and Karamanis & Hodes (2016), whereby the advection (left-hand side) in (2.21) is assumed known from the previous iteration. In this way, the problem to update  $\phi$  is linear and decoupled from  $\lambda$ , which is subsequently updated using (2.33). Convergence is very rapid, with less than 10 iterations required to achieve a relative change in  $\lambda$  of less than 0.01%.

Convergence of the spatial discretisation was confirmed by doubling N and M until  $\lambda$  changed by less than 0.5%. For all of the results shown, typically N=20 was sufficient, with M chosen as follows. Since we are concerned with small spacing-to-height ratios  $\varepsilon$ , we found it important to increase M (vertical grid points per subdomain) as  $\varepsilon$  decreases. Indeed, we related M to N via the scaling  $M=N/(2\varepsilon)$ , until a maximum value of M=100. This led to good results down to an  $\varepsilon$  value of 0.025. To decrease  $\varepsilon$  further without unreasonable computational effort, one could introduce additional subdomains (e.g. close to the fin tip) to cluster the grid points more efficiently, or instead subtract the local form of the singularity at (x, y) = (0, 1) (as in Game  $et\ al.\ 2018$ ). However, this was not the focus of our study.

The numerical results for Nu were compared (see figure 9) with those of Sparrow *et al.* (1978), with differences of the order of one per cent or less – the discrepancies likely due to the coarser mesh of Sparrow *et al.* (1978) (who took at most 50 equally spaced points in the y direction).

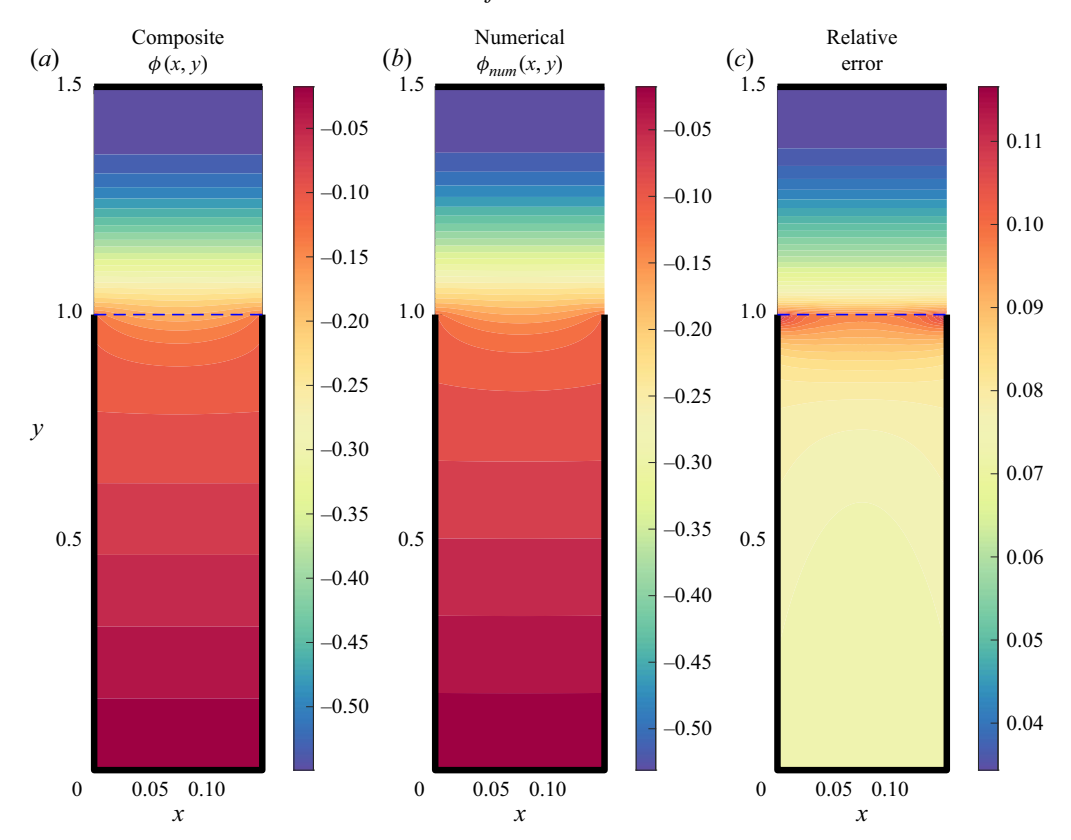


Figure 4. The asymptotic piece-wise composite solution (3.47)–(3.48) for the scaled temperature field  $\phi(x, y) = T/\lambda$  in one period (a), compared with the numerical temperature (b), with the local relative error  $|\phi(x, y) - \phi_{num}(x, y)|/|\phi_{num}|$  (c). Here,  $\varepsilon = 0.15$ , c = 0.5, and  $\Omega = 1$ . See caption for figure 3.

# 5.2. Velocity and temperature fields: $w(x, y), \phi(x, y)$

We begin by comparing the asymptotic composite solutions for w(x, y) ((3.17)–(3.18)) and  $\phi(x, y)$  ((3.47)–(3.48)) with the numerical solutions. Figure 3 compares w(x, y) for the case  $\varepsilon = 0.15$  (on the upper end of the practical range) and c = 0.5. The structure of the flow is captured excellently by the asymptotic solution: the bulk of the flow occurs above the fins in an almost parabolic profile, and only weakly penetrates down into the space between the fins (where the velocity is an order of magnitude lower). The composite is actually discontinuous on the line y = 1, due to there being  $O(\varepsilon^2)$  terms in y < 1 and not in  $y \ge 1$ , but this discontinuity is still small, as expected.

Figure 4 compares  $\phi(x, y)$  for the same geometry, and for a fin conductivity parameter  $\Omega=1$ . We show here the scaled temperature  $\phi$ , not the 'non-dimensional temperature' T, which is related via  $T=\lambda\phi$ . This was done in an attempt to compare the temperature distributions. The overall magnitude is affected greatly by the approximation to  $\lambda$ , which we assess separately. (Note that T is positive but  $\lambda$  is negative and so  $\phi$  is negative). As per figure 4, the field structure is captured, where the heat transfer is predominantly one-dimensional (1-D) conduction from the base until close to the fin tips where the conduction becomes two-dimensional (from the fin to the fluid), followed by a 1-D convection behaviour (and nonlinear temperature profile) above the fins. The relatively low value of the fin conductivity parameter,  $\Omega=1$ , was chosen to exhibit the 1-D conduction clearly, but in practice  $\Omega$  will generally be larger (Karamanis & Hodes 2019a). There is a

#### T.L. Kirk and M. Hodes

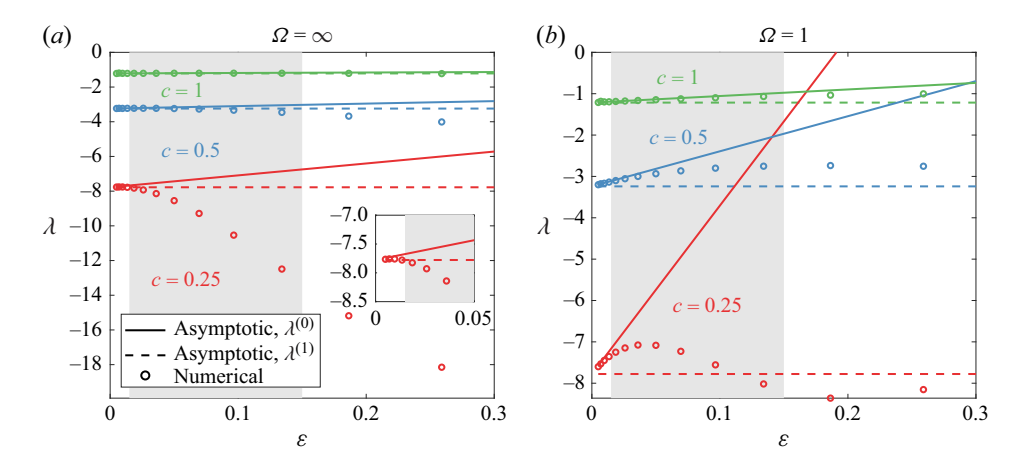


Figure 5. The solution constant  $\lambda$ , comparing the asymptotic solutions for  $\varepsilon \ll 1$  to the numerical solution. Dashed lines are using only the leading order (3.44) and solid lines are the full (two term) approximation (3.45). Shaded region shows the realistic range  $0.015 < \varepsilon < 0.15$  of fin spacings applicable to manufacturable heat sinks (Iyengar & Bar-Cohen 2007). Inset in (a) shows a zoom in close to  $\varepsilon = 0$ .

rather uniform relative error throughout the fin region, reflecting a small error (order  $\varepsilon^2$ ) in the heat flux up the fin. The error is overall small (typically  $\lesssim 7$  %), and is greatest in the tip region due to error in the fin tip temperature combined with error due to neglected advection. Unlike the velocity composite, the temperature composite is continuous at y=1.

#### 5.3. The constant $\lambda$

In this section we compare the asymptotic approximation(s) for the solution constant  $\lambda$  with the numerical solution. Recall that  $\lambda$  can be interpreted as the exponential decay rate in the streamwise direction (z) of the (self-similar) temperature profile towards the isothermal base temperature. It also directly gives the overall Nusselt number (4.9). Figure 5 compares two approximations for  $\lambda$  against numerical solutions for a range of  $\varepsilon$  (down to  $\varepsilon=0.025$ ), and selected c and  $\Omega$  values. In all cases, the approximation  $\lambda^{(0)}$  captures the limiting value of  $\lambda_{num}$  as  $\varepsilon\to 0$  (as it should), and  $\lambda^{(1)}$  captures the value and slope (as it should). However, even though the slope is captured, as c decreases it is clear that the range of  $\varepsilon$  for which  $\lambda^{(1)}$  is a good approximation also decreases. This is expected, since the asymptotic approximation requires  $\varepsilon\ll 1$  but also  $\varepsilon\ll c$ , i.e. that the fin spacing is small compared with the clearance. Hence the assumption breaks down if, e.g.  $c=O(\varepsilon)$  (as seen for f Re in Miyoshi et al. 2024), as is clear from (3.45) since the correction is proportional to  $\varepsilon/c$ . Additionally, the accuracy of  $\lambda^{(1)}$  decreases as  $\Omega$  decreases, also seen from the correction.

Indeed, from the expansion (3.45) one can summarise the validity requirements as  $\varepsilon/c\ll 1$  and  $\varepsilon/(c\Omega)\ll 1$ , since otherwise the correction is comparable to the leading term. The first condition,  $\varepsilon/c\ll 1$ , is purely a geometric requirement necessary for there to be a gap region above the fins where the flow and temperature depends only on y. The second condition,  $\varepsilon/(c\Omega)\ll 1$ , is a further constraint that applies to the conductivity of the fin. The leading-order temperature in the fin is  $T_f=-\hat{\lambda}_0\varepsilon y/(c\Omega)+\cdots$ , implying that the dimensionless temperature drop  $\Delta T_f$  across the height of the fin is  $\Delta T_f\sim\varepsilon/(c\Omega)$ . Hence the constraint above implies  $\Delta T_f\ll 1$ , or in dimensional terms,

$$T_{base}^* - T_{f, tip}^* \ll T_{base}^* - T_b^*,$$
 (5.1)

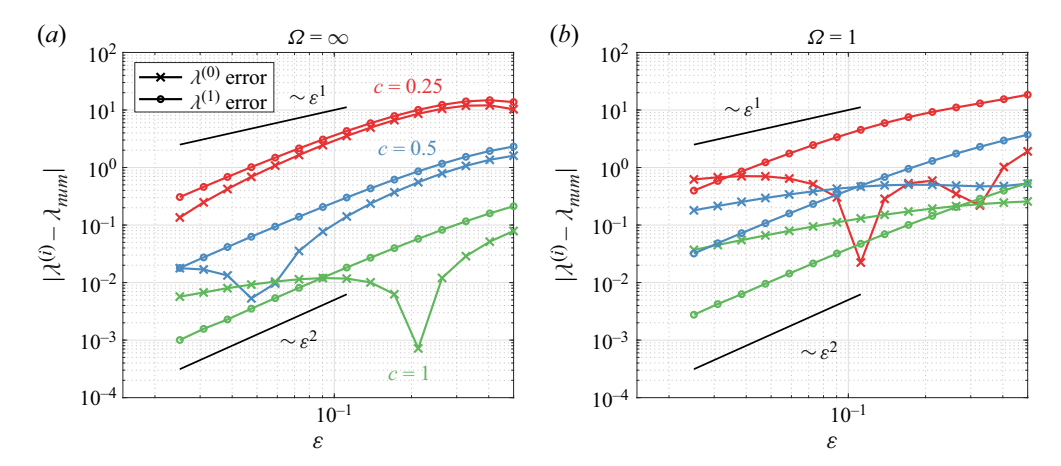


Figure 6. Absolute error of the asymptotic approximations for the constant  $\lambda$ , compared with the numerical solution. The error is shown for two levels of approximation,  $\lambda^{(0)} = \lambda_0$  and  $\lambda^{(1)} = \lambda_0 + \varepsilon \lambda_1$ . Values of c and  $\Omega$  are indicated.

i.e. the temperature drop from the base to the fin tip is small compared with the drop from the base to the fluid bulk. If the dimensionless fin conductivity is not high enough (due to solid/fluid conductivity or fin thickness) then the temperature at the tip of the fin becomes comparable to the bulk temperature  $T_b^*$ . Then the heat transfer between the fin and the bulk cannot predominantly occur near the tip: a significant portion must also occur further down the fin – and thus advection there (not just in the gap region above) would need to be considered. To summarise, the condition  $\Delta T_f = \varepsilon/(c\Omega) \ll 1$  can be viewed as a refinement on the initial assumption (which was that  $\Omega = O(1)$  or larger) to the extended range  $\Omega \gg \varepsilon/c$ . When this is violated, advection between the fins is not negligible.

Moving on, a surprising result is the accuracy of the leading-order solution  $\lambda^{(0)}$ . When the fins are highly conductive (say  $\Omega = \infty$ , figure 5a),  $\lambda^{(0)}$  and  $\lambda^{(1)}$  are similar approximations, but  $\lambda^{(0)}$  is slightly closer (for larger  $\varepsilon$ ) to the numerics as c is decreased. This is further exaggerated as the fins become less conductive (figure 5b). Mathematically, it is clear that this is due to the strong non-monotonic dependence of  $\lambda$  on  $\varepsilon$ : the better accuracy of  $\lambda^{(1)}$  for small  $\varepsilon$  results in worse accuracy for larger  $\varepsilon$ . However, this significant advantage of  $\lambda^{(0)}$  over  $\lambda^{(1)}$  seems to occur mainly outside of the realistic range of fin spacings (0.015 <  $\varepsilon$  < 0.15), shown in grey.

The above points are made more apparent by looking at the absolute error of  $\lambda^{(0)}$  and  $\lambda^{(1)}$  in figure 6. The errors of  $\lambda^{(0)}$  and  $\lambda^{(1)}$  show slopes of 1 (indicating  $O(\varepsilon)$ ) and 2 (indicating  $O(\varepsilon^2)$ ), respectively, as  $\varepsilon \to 0$ . For moderately large  $\varepsilon$ ,  $\lambda^{(0)}$  typically shows the smaller error, but below some critical value of  $\varepsilon$  (which increases with c),  $\lambda^{(1)}$  always becomes more accurate. This has consequences for the  $\overline{Nu}$  approximations, discussed in § 5.5.

# 5.4. Local Nusselt number on the fin surface

In this section we assess the approximation of local quantities along the surface of the fin. We begin with the local Nusselt number  $Nu_f$ , given numerically by definition (4.1), and approximated by (4.3). Figure 7 compares (the absolute value of)  $Nu_f$  for a range of  $\varepsilon$ , c and  $\Omega$  values. It is plotted in terms of the tip variable Y, and the behaviour is reminiscent of that in Sparrow *et al.* (1978). Our formula shows that it is singular  $(Nu_f = O(|Y|^{-1/2}))$  as  $Y \to 0$ , and decays very quickly  $(Nu_f = O(e^{-\pi|Y|}))$  as you move away from the tip,  $Y \to -\infty$ . The singularity is expected from the change of thermal boundary condition

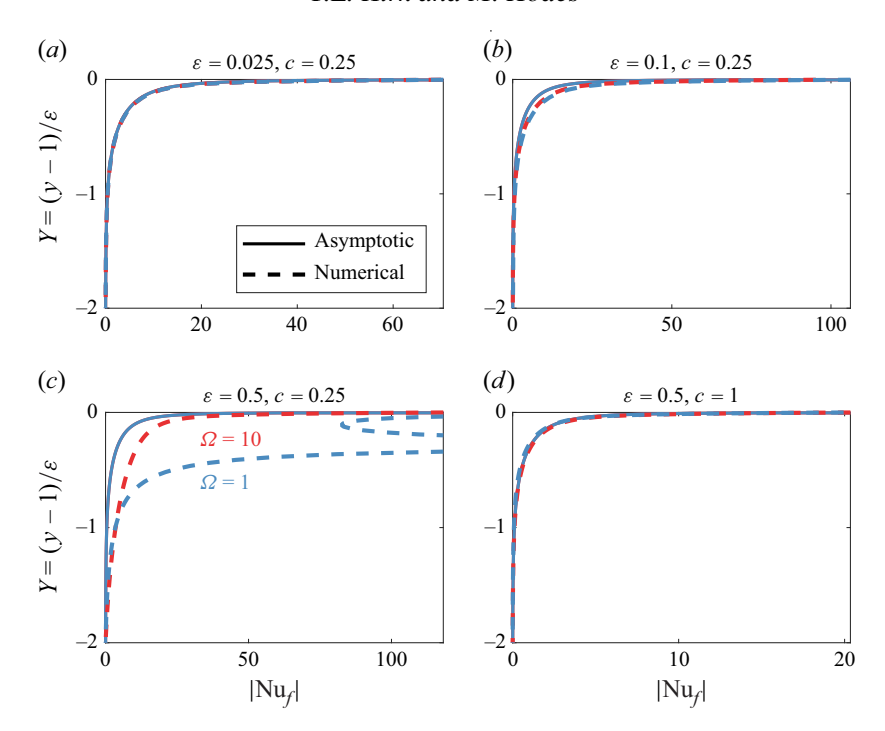


Figure 7. The (magnitude of) local Nusselt number on the fin surface,  $Nu_f(Y)$  as a function of the tip variable  $Y = (y-1)/\varepsilon$ , comparing asymptotic (given by 4.3) and numerical solutions. The values of c,  $\varepsilon$  and  $\Omega$  are indicated. Different solutions are only distinguishable in (b), (c).

there from a Dirichlet one  $(T=T_f, y<1)$  to a Neumann one  $(\partial T/\partial x=0, y>1)$ , and the asymptotic solution captures the behaviour excellently. Indeed, the shape barely changes as the parameters are varied (its magnitude scales with c), only when the asymptotic assumption breaks down, i.e. the case  $c=0.25<\varepsilon=0.5$ . As remarked by Sparrow et al. (1978), this behaviour is very far from the common assumption of a 'constant heat transfer coefficient' along the fin surface, and it is consistent across parameters, even when the fin conductivity is low ( $\Omega=1$ ). In fact,  $Nu_f$  often becomes negative close to the tip (see the case  $\Omega=1$  in figure T(c), but note that only the magnitude is plotted), and increasing  $\Omega$  (by increasing fin thickness) might not be optimal for a heat sink since overall surface area is lost.

The non-dimensional temperature  $T_f = (T_f^* - T_{base}^*)/(T_b^* - T_{base}^*)$ , for the same parameter cases, is shown in figure 8. The linear 1-D conduction behaviour in y, exhibited by the asymptotic solution (3.23), is observed in most cases. It departs from linear close to the tip (y=1), in a small region that widens with  $\varepsilon$ . The agreement worsens as  $\varepsilon$  increases, and c or  $\Omega$  decreases. Note that we used the leading-order approximation for  $\lambda = \lambda_0 + \ldots$  here, since moderate accuracy for a wider range of  $\varepsilon$  was necessary for illustration.

#### 5.5. Overall Nusselt number $\overline{Nu}$

Finally, we compare the approximations for the overall Nusselt number Nu, which gives a measure of the overall efficacy of the heat transfer to the fluid. We note that  $\overline{Nu}$  and fRe (provided by Miyoshi *et al.* 2024), are necessary to calculate the thermal resistance of the heat sink (Karamanis & Hodes 2016). Figure 9 compares (4.10)–(4.11) with the numerical solutions for the same parameters as in figure 5. Since  $\overline{Nu}$  follows directly from  $\lambda$ ,

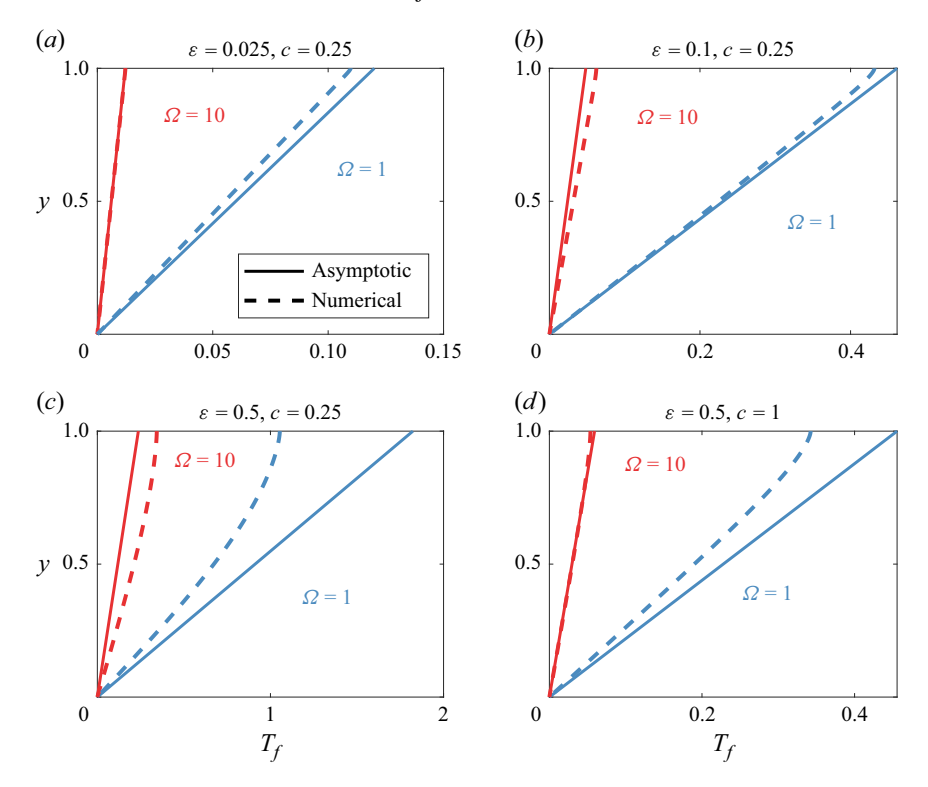


Figure 8. The temperature along the fin  $T_f(y)$  comparing the numerical solution (spectral collocation), and the asymptotic solution  $T_f \sim \lambda_0 \tilde{\phi}_f$  in the fin region ( $0 \le y$  and  $1 - y \gg \varepsilon$ ), where  $\tilde{\phi}_f$  is (3.23). The values of c,  $\varepsilon$  and  $\Omega$  are indicated.

the approximations exhibit similar behaviour and regions of validity as those for  $\lambda$ , but most notably  $\overline{Nu}$  contains an additional factor of  $\varepsilon$  and thus  $\overline{Nu} \to 0$  as  $\varepsilon \to 0$ . Similar to  $\lambda$ , both approximations show good agreement with the numerics, but  $\overline{Nu}^{(1)}$  shows excellent agreement for smaller values of  $\varepsilon$ , and  $\overline{Nu}^{(0)}$  shows moderate agreement over a larger range of  $\varepsilon$ . Notably,  $\overline{Nu}^{(0)}$  remains positive whereas  $\overline{Nu}^{(1)}$  can erroneously become negative far outside its range of validity.

The values of  $\overline{Nu}$  here in the realistic  $\varepsilon$  range are remarkably low compared with the typical values without tip clearance (c=0), where  $\overline{Nu}\approx 2-34$  (Sparrow *et al.* 1978). Thus, to avoid gross overestimation, it is crucial to not use such values when there is tip clearance, but the formulas provided here instead.

The accuracy of  $\overline{Nu}^{(1)}$  is perhaps better shown in figure 10 where the relative error is plotted in the  $(c, \varepsilon)$ -plane for  $\varepsilon \in [0.025, 0.5]$ ,  $c \in [0.025, 1]$ . Error is lowest when  $\varepsilon$  is small and c and  $\Omega$  are large, consistent with the asymptotic requirements that  $\varepsilon/c \ll 1$  and  $\varepsilon/(c\Omega) \ll 1$ . Also shown are black marginal lines, to the left of which, the relative error is less than 5 % or 15 %. For the range plotted, the error of  $\overline{Nu}^{(1)}$  was found to be < 15 % in the following approximate region (provided  $\Omega \geqslant 1$ ):

$$c \geqslant 4.2\varepsilon + 0.06. \tag{5.2}$$

For completeness, we also plot the error of  $\overline{Nu}^{(0)}$  in figure 11. The behaviour is far less predictable, but the regions where the error is < 15 % are generally larger than for  $\overline{Nu}^{(1)}$ .

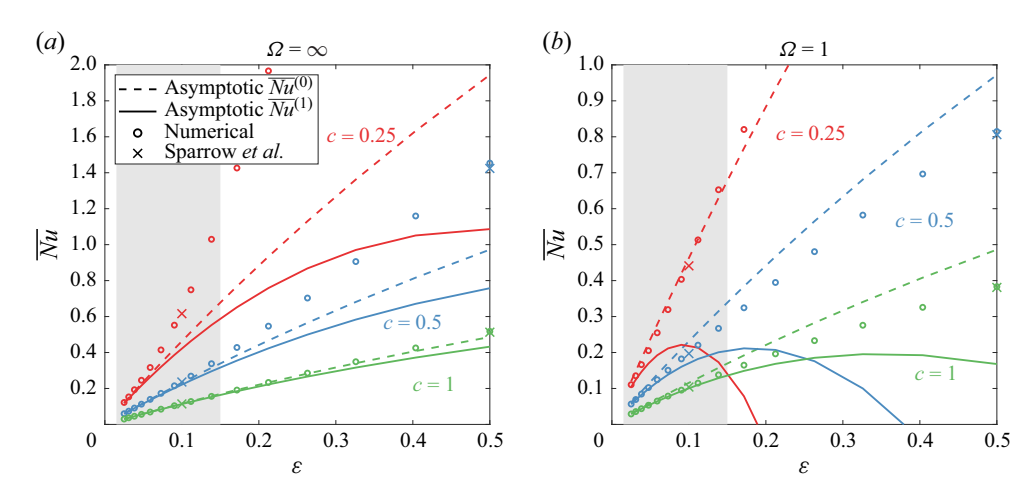


Figure 9. The overall average Nusselt number  $\overline{Nu}$ , comparing the asymptotic solutions (4.10)–(4.11) for  $\varepsilon \ll 1$  with the numerical solution. Values from Sparrow *et al.* (1978) are also shown, where available. Shaded region shows the realistic range  $0.015 < \varepsilon < 0.15$  applicable to manufacturable heat sinks.

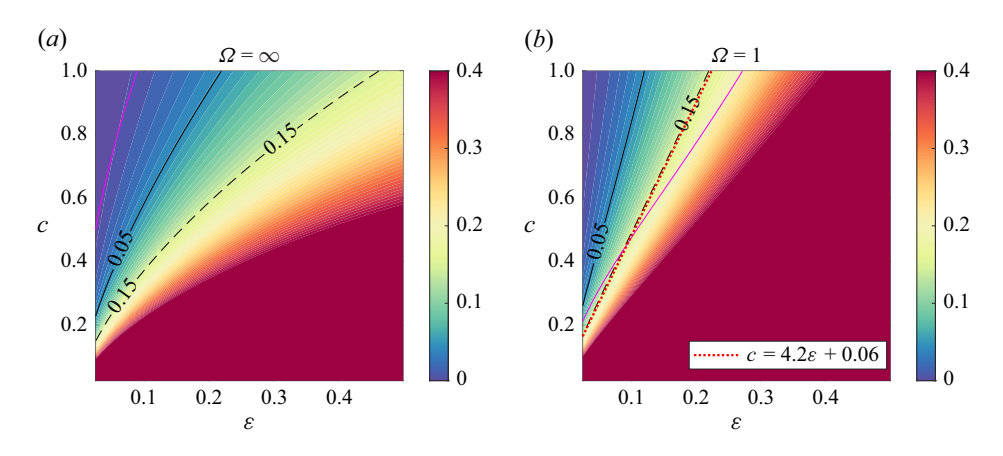


Figure 10. Relative error of approximation  $\overline{Nu}^{(1)}$  (see (4.11)), compared with the numerical solution, i.e. contours of  $|\overline{Nu}^{(1)} - \overline{Nu}_{num}|/\overline{Nu}_{num}$  for  $\varepsilon \in [0.025, 0.5]$ ,  $c \in [0.025, 1]$ . The marginal boundaries where the error is 0.05 and 0.15 (5% and 15%) are shown as black lines and labelled. The magenta line indicates a boundary, above which  $\overline{Nu}^{(1)}$  is more accurate than  $\overline{Nu}^{(0)}$ .

In particular, when  $\Omega=1$  and 0.2 < c < 0.4, this region extends up to  $\varepsilon < 0.45$ . Hence,  $\overline{Nu}^{(0)}$  can have particular use cases over  $\overline{Nu}^{(1)}$ , but these cases may be difficult to predict and require trial and error to determine. It may be useful to know when one should use  $\overline{Nu}^{(1)}$  over  $\overline{Nu}^{(0)}$ , and this is indicated by the magenta line in figures 10 and 11, above which  $\overline{Nu}^{(1)}$  is more accurate and should be used.

# 6. Conclusions

In this paper, we considered the convective heat transfer problem for a LFHS (isothermal base) with tip clearance – a classic and ubiquitous problem in the thermal management of electronics. We considered an analytical approach to the mathematical problem formulated

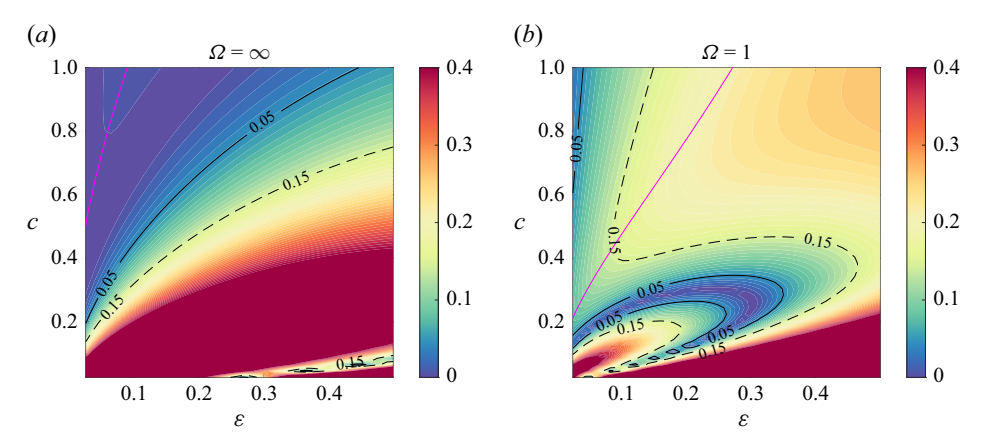


Figure 11. Relative error of approximation  $\overline{Nu}^{(0)}$  (4.10). See caption for figure 10.

and solved numerically by Sparrow *et al.* (1978). In particular, we presented a detailed asymptotic solution for the flow and (coupled, i.e. conjugate) temperature fields in the fluid and the fins, in the limit of small fin spacing,  $\varepsilon \ll 1$ .

We used the method of matched asymptotic expansions, and decomposed the flow domain into regions where different transport processes are important: (i) a gap region (above the fins) where the flow is the fastest but one-dimensional, driving a 1-D convection profile; (ii) a tip region (close to the fin tips) where the flow and temperature fields are two-dimensional (and purely diffusive); (iii) a fin region (down between the fins) where the flow is almost stagnant, and so the thermal problem is purely 1-D conduction and governed by relative conductivity of the fin. The structure elaborates on the insights of Sparrow et al. (1978) on why the heat transfer suffers when there is clearance. Because the heat transfer predominantly occurs close to the fin tips, the use of uniform heat transfer coefficients is wholly inappropriate: instead, the local coefficient is singular at the tip and decays to a negligible value after approximately 1 fin spacing from the tip. This has practical implications on the design of unshrouded heat sinks for low-power components in circuit packs. First, the fins need not be much taller than the spacing between them – a maximum height of 2 times the fin spacing would be sufficient due to the lack of flow close to the base. Secondly, the fins may be extremely thin but maintain very high fin efficiency as their tips are so close to their base.

The 1-D convection problems in the gap region at each order only need to be solved once, and this is trivially done numerically. Remarkably, explicit solutions are found for the local heat transfer coefficient (or Nusselt number  $Nu_f$ ); the fin and fluid temperature throughout the entire fin and tip regions; the heat flux along the length of the fin; and the overall Nusselt number  $(\overline{Nu})$ . Therefore, one does not have to rely purely on numerical solutions, or crude (and inaccurate) uniform assumptions, for this relevant heat transfer problem anymore. These solutions are compared with numerical solutions of the full coupled problem for arbitrary  $\varepsilon$  and are found to agree well for small  $\varepsilon$  in the realistic range  $(0.015 \leqslant \varepsilon \leqslant 0.15)$ . In general, they are valid under the parametric assumptions  $\varepsilon \ll 1$ ,  $\varepsilon/c \ll 1$  and  $\varepsilon/(c\Omega) \ll 1$ . The first two are geometric assumptions, and the third ensures that the temperature drop along the fin is small compared with the overall driving temperature difference between the base  $(T_{base}^*)$  and the fluid bulk  $(T_b^*)$ . Thus, accuracy decreases if  $\varepsilon$  increases, c decreases, or  $\Omega$  decreases.

The leading-order formula for the overall heat transfer  $(\overline{Nu})$  shows good accuracy for a moderate range of  $\varepsilon$ . The higher-order formula gives better accuracy when  $\varepsilon$  is small (i.e. in

the realistic range), but at the expense of worse accuracy for moderate  $\varepsilon$ . Nonetheless, the error of the higher-order formula was found to be < 15 % for all  $\varepsilon$  we considered, provided the modest conditions  $c \ge 4.2\varepsilon + 0.06$  and  $\Omega \ge 1$ .

We focused here on the scenario with tip clearance (c>0). The case where the heat sink is fully shrouded, without tip clearance (c=0) is another very relevant one. The transport structure is significantly different since the location of highest flow velocity occurs between the fins, and hence advection there appears at leading order and cannot be neglected. The solution is thus not simply the limit  $c\to 0$  of the solution presented here. The c=0 case will be published in future work.

In summary, our companion paper by Miyoshi *et al.* (2024) provided analytical results for the Poiseuille number through rectangular ducts with two (facing) surfaces having mixed (no-slip and shear-free) boundary conditions, which previously had not been done. Extending this configuration to a diabatic problem, the present study provides analytical results for conjugate Nusselt numbers through such ducts having (facing) surfaces where the conjugate heat transfer problem has been resolved. These analytical formulas (Poiseuille numbers from Miyoshi *et al.* (2024) and Nusselt numbers from the present study) could enable the thermal resistance optimisation of a LFHS, done numerically in Karamanis & Hodes (2016), to be performed more easily.

Supplementary material. Supplementary material is available at https://doi.org/10.1017/jfm.2025.10417.

**Funding.** T.L.K. was supported in part by a Chapman Fellowship in the Department of Mathematics, Imperial College London.

Declaration of interests. The authors report no conflict of interest.

# Appendix A. Derivation of the temperature solution in the small-fin-spacing limit $\varepsilon \to 0$

In this appendix, we give the derivation of the temperature solution presented in § 3.2. Rescaling  $x = X/\varepsilon$ , the problem for  $\phi$  is

$$\lambda \mathcal{W}\phi = \frac{1}{\varepsilon^2} \frac{\partial^2 \phi}{\partial X^2} + \frac{\partial^2 \phi}{\partial y^2} \quad \text{in } \mathcal{D},\tag{A1}$$

$$\phi = 0 \qquad \text{on } y = 0, \tag{A2}$$

$$\frac{\partial \phi}{\partial y} = 0$$
 on  $y = 1 + c$ , (A3)

$$\frac{\partial \phi}{\partial X} = 0 \qquad \text{on } X = 0, \quad 1 < y < 1 + c, \tag{A4}$$

$$\frac{\partial \phi}{\partial X} = 0 \qquad \text{on } X = 1/2, \quad 0 < y < 1 + c, \tag{A5}$$

in the fluid, and

$$\varepsilon \Omega \frac{\mathrm{d}^2 \phi_f}{\mathrm{d}y^2} = -\left. \frac{\partial \phi}{\partial X} \right|_{X=0}, \quad \text{for } 0 < y < 1,$$
 (A6)

$$\phi_f = \phi|_{X=0}$$
, for  $0 < y < 1$ , (A7)

$$\phi_f = 0, \quad \text{at } y = 0, \tag{A8}$$

$$\frac{\mathrm{d}\phi_f}{\mathrm{d}y} = 0, \quad \text{at } y = 1, \tag{A9}$$

in the fin, with decay constant

$$\lambda = \frac{1+c}{\int_0^1 \int_0^{1+c} \mathcal{W}\phi \, \mathrm{d}y \mathrm{d}X}.$$
 (A10)

A.1. *Gap region:* 
$$1 < y \le 1 + c$$

Given  $\phi = 0$  on the base, we expect  $\phi$  to have the largest magnitude in the gap region, furthest from the heat transport surfaces. If we anticipate a balance between conduction in the y-direction and streamwise advection, then  $\partial^2 \phi / \partial y^2 \sim \lambda W \phi$ . But W = O(1) in the gap region and  $\lambda = O(1/\phi)$  from (A10), and thus  $\partial^2 \phi / \partial y^2 = O(1)$ . This gives the leading order estimate that  $\phi = O(1)$  and  $\lambda = O(1)$  as  $\varepsilon \to 0$ . Considering expansions

$$\phi = \phi_0 + \varepsilon \phi_1 + O(\varepsilon^2), \tag{A11}$$

$$\lambda = \lambda_0 + \varepsilon \lambda_1 + O(\varepsilon^2),\tag{A12}$$

$$W = W_0(y) + \varepsilon W_1(y) + O(\varepsilon^2), \tag{A13}$$

similar arguments to those for the velocity field in the gap region follow here and we find that  $\phi_0(y)$ ,  $\phi_1(y)$  depend on y only. At leading order,  $\phi_0(y)$  satisfies the one-dimensional problem

$$\lambda_0 \mathcal{W}_0(y) \phi_0 = \frac{d^2 \phi_0}{dy^2} \quad \text{in } 1 < y < 1 + c,$$
 (A14)

$$\frac{\mathrm{d}\phi_0}{\mathrm{d}y} = 0 \qquad \text{on } y = 1 + c, \tag{A15}$$

$$\lambda_0 = \frac{1+c}{\int_1^{1+c} W_0(y)\phi_0(y) \, dy},$$
 (A16)

and at first order,  $\phi_1(y)$  satisfies

$$(\lambda_1 \mathcal{W}_0 + \lambda_0 \mathcal{W}_1)\phi_0 + \lambda_0 \mathcal{W}_0 \phi_1 = \frac{d^2 \phi_1}{dy^2} \quad \text{in } 1 < y < 1 + c,$$
 (A17)

$$\frac{\mathrm{d}\phi_1}{\mathrm{d}y} = 0 \qquad \text{on } y = 1 + c, \tag{A18}$$

$$\lambda_1 = -\frac{\lambda_0^2}{1+c} \int_1^{1+c} (\mathcal{W}_0 \phi_1 + \mathcal{W}_1 \phi_0) \, \mathrm{d}y. \tag{A19}$$

Note, since the velocity  $W = O(\varepsilon)$  and  $O(\varepsilon^2)$  in the tip  $(y - 1 = O(\varepsilon))$  and fin regions (0 < y < 1), the contributions of those regions to the integral for  $\lambda$  appear at  $O(\varepsilon^2)$  and hence are ignored.

These problems for  $\phi_0$  and  $\phi_1$  also have a matching condition with the tip region as  $y \to 1^+$ , which are yet to be determined. The problems for  $\phi_0$  and  $\phi_1$  with these conditions included are detailed in the summary, § 3.2.

#### T.L. Kirk and M. Hodes

A.2. Fin region: 
$$0 \le y < 1$$

In the fin region, we must solve for the fluid temperature but also the fin temperature  $\phi_f(y)$ . Denoting the fluid temperature here by  $\tilde{\phi}$ , and expanding both temperatures as

$$\tilde{\phi} = \tilde{\phi}_0 + \varepsilon \tilde{\phi}_1 + O(\varepsilon^2), \tag{A20}$$

$$\phi_f = \phi_{f0} + \varepsilon \phi_{f1} + O(\varepsilon^2), \tag{A21}$$

and noting that the advection terms are  $O(\varepsilon^2)$  at most (since  $W = O(\varepsilon^2)$  here), at leading order in (A1), (A5) and (A6) we find (where (A6) gives the condition at X = 0).

$$\frac{\partial^2 \tilde{\phi}_0}{\partial X^2} = 0 \tag{A22}$$

$$\frac{\partial \tilde{\phi}_0}{\partial X} = 0, \quad \text{at } X = 0, 1/2 \tag{A23}$$

and so integrating the former and applying the latter gives that  $\tilde{\phi}_0(y)$  is a function of y only, and matches the fin temperature by continuity,  $\phi_{f0}(y) = \tilde{\phi}_0(y)$ . At the next order,  $O(\varepsilon^{-1})$  in (A1) and  $O(\varepsilon)$  in (A6), we have

$$\frac{\partial^2 \tilde{\phi}_1}{\partial X^2} = 0,\tag{A24}$$

$$\Omega \frac{\mathrm{d}^2 \phi_{f0}}{\mathrm{d}y^2} = -\left. \frac{\partial \tilde{\phi}_1}{\partial X} \right|_{X=0}, \quad \text{for } 0 < y < 1.$$
 (A25)

Integrating (A24), and applying symmetry about the midline X = 1/2 then  $\tilde{\phi}_1(y)$  is also only a function of y, with  $\phi_{f1}(y) = \tilde{\phi}_1(y)$  by continuity. Then the right-hand side of (A25) vanishes; no heat is conducting out of the fin at this order in this region. Integrating (A25) and applying the isothermal condition  $\phi_{f0} = 0$  at the base y = 0, we get

$$\phi_{f0}(y) = \tilde{\phi}_0(y) = \Delta_0 y, \tag{A26}$$

where  $\Delta_0$  is a constant to be determined. Going to the next order,  $O(\varepsilon^0)$  in (A1) and  $O(\varepsilon^2)$  in (A6), similar arguments give that

$$\phi_{f1}(y) = \tilde{\phi}_1(y) = \Delta_1 y, \tag{A27}$$

for a constant  $\Delta_1$ . We cannot apply the boundary condition (A9) at the ridge tip y=1 at each order since the assumption that the fluid temperature ( $\tilde{\phi}_0$  and  $\tilde{\phi}_1$ ) is independent of X breaks down there. Hence, we must match with a solution in the tip region. Nonetheless, it is surprising that there is no conduction out of (the majority of) the fin into the fluid at the first two orders of the expansion; conduction is purely one-dimensional and in the y direction.

A.3. Tip region: 
$$y - 1 = O(\varepsilon)$$

Estimates from the gap and fin region solutions as  $y \to 1$  are that the temperatures, denoted here by  $\phi = \Phi$  and  $\phi_f = \Phi_f$ , are O(1). Substituting  $y = 1 + \varepsilon Y$  into (A1)–(A9), and noting

that  $W \sim \varepsilon W_1/\overline{w} = O(\varepsilon)$  here, we find

$$\nabla_{XY}^2 \Phi = O(\varepsilon^3) \quad \text{in } \mathcal{D}_{tip} = \{0 < X < 1/2, \ -\infty < Y < \infty\},$$
 (A28)

$$\frac{\partial \Phi}{\partial X} = 0$$
 on  $X = 0$ ,  $0 < Y$ , (A29)

$$\frac{\partial \Phi}{\partial X} = 0$$
 on  $X = 1/2$ ,  $-\infty < Y < \infty$ , (A30)

in the fluid, and

$$\Omega \frac{\mathrm{d}^2 \Phi_f}{\mathrm{d}Y^2} = -\varepsilon \left. \frac{\partial \Phi}{\partial X} \right|_{X=0}, \quad \text{for } Y < 0, \tag{A31}$$

$$\Phi_f = \Phi|_{X=0} , \quad \text{for } Y < 0, \tag{A32}$$

$$\frac{\mathrm{d}\Phi_f}{\mathrm{d}Y} = 0, \quad \text{at } Y = 0, \tag{A33}$$

in the fin. Expanding as per

$$\Phi = \Phi_0 + \varepsilon \Phi_1 + O(\varepsilon^2), \tag{A34}$$

$$\Phi_f = \Phi_{f0} + \varepsilon \Phi_{f1} + O(\varepsilon^2), \tag{A35}$$

then  $\Phi_{f0}$  satisfies  $d^2\Phi_{f0}/dY^2 = 0$ , which integrated with the application of boundary condition (A33) implies that  $\Phi_{f0}$  is a constant. Matching (as  $Y \to -\infty$ ) with the fin region solution (as  $y \to 1^-$ ) at leading order means

$$\Phi_{f0} \to \Delta_0$$
, as  $Y \to -\infty$ , (A36)

and hence  $\Phi_{f0} \equiv \Delta_0$ . With the fin isothermal, the fluid temperature  $\Phi_0$  satisfies  $\nabla^2_{XY} \Phi_0 = 0$  in the strip, with  $\Phi_0 = \Delta_0$  on the fin (Y < 0), symmetry above the fins (Y > 0), and matching conditions

$$\Phi_0 \to \phi_0(y=1^+), \quad \text{as } Y \to \infty,$$
 (A37)

$$\Phi_0 \to \Delta_0$$
, as  $Y \to -\infty$ , (A38)

with the gap and fin regions, respectively. However, the problem for  $\Phi_0 - \Delta_0$  is identical in form to the velocity problem  $W_0$  in this region, which was found to be identically zero (Miyoshi *et al.* 2024). Therefore,  $\Phi_0 \equiv \Delta_0$  and  $\phi_0(y=1^+) = \Delta_0$ , with  $\Delta_0$  still unknown.

Proceeding to the next order, the fin temperature correction  $\Phi_{f1}$  satisfies  $d^2\Phi_{f1}/dY^2=0$ . Integrating and applying (A33) implies that  $\Phi_{f1}$  is also a constant. The matching condition with the fin region solution at  $O(\varepsilon)$  means

$$\Phi_{f1} \sim \Delta_0 Y + \Delta_1 \quad \text{as } Y \to -\infty,$$
 (A39)

but as  $\Phi_{f1}$  is constant, this is possible only if  $\Delta_0 = 0$ , giving  $\Phi_{f1} \equiv \Delta_1$ . The leading-order fin and fluid temperatures are thus actually  $O(\varepsilon)$ . Also, since  $\Delta_0 = 0$ , the matching condition for the gap solution is now

$$\phi_0 = 0$$
 at  $y = 1^+$ . (A40)

The problem for  $\Phi_1$  follows from (A28)–(A30), (A32) as

$$\nabla_{XY}^2 \Phi_1 = 0 \quad \text{in } \mathcal{D}_{tip}, \tag{A41}$$

$$\frac{\partial \Phi_1}{\partial X} = 0 \qquad \text{on } X = 0, 1, \quad 0 < Y, \tag{A42}$$

$$\Phi_1 = \Delta_1$$
 on  $X = 0, 1, Y < 0,$  (A43)

with matching condition to the fin region

$$\Phi_1 \to \Delta_1 \quad \text{as } Y \to -\infty.$$
 (A44)

For the matching condition (as  $Y \to +\infty$ ) with the gap region, it is convenient to derive one for the heat flux. Integrating the leading-order gap equation (A14) across the gap 1 < y < 1 + c and using (A15), (A16), we find

$$\frac{d\phi_0}{dy} = -(1+c), \quad \text{at } y = 1^+.$$
 (A45)

Doing the same for the first-order equation (A17), we find

$$\frac{d\phi_1}{dy} = 0$$
, at  $y = 1^+$ . (A46)

Transforming to the tip variable  $Y = (y - 1)/\varepsilon$ , this gives the matching condition on  $\Phi_1$ 

$$\frac{\partial \Phi_1}{\partial Y} \to -(1+c) \quad \text{as } Y \to \infty,$$
 (A47)

or 
$$\Phi_1 \sim -(1+c)Y$$
 as  $Y \to \infty$ . (A48)

Notice now that the problem (A41)–(A44), (A48), when considered as a problem for the difference  $\Phi_1 - \Delta_1$ , is identical to the problem for  $W_1$  (see (3.10)–(3.14)), but with a 'shear rate' of -(1+c) as  $Y \to \infty$  instead of c/2. Therefore, remarkably, the same solution can be used here for the thermal problem, and it is given by

$$\Phi_1 = \Delta_1 - \frac{2(1+c)}{c} W_1(X,Y), \tag{A49}$$

$$= \Delta_1 + \frac{1+c}{\pi} \log \left| \frac{e^{i\pi/4} - \tan^{1/2}(\pi Z/2)}{e^{i\pi/4} + \tan^{1/2}(\pi Z/2)} \right|, \quad \text{where } Z = X + iY, \quad (A50)$$

with far-field behaviour

$$\Phi_1 \sim -(1+c) \left[ Y + \frac{\log 2}{\pi} - \frac{\Delta_1}{1+c} + O(e^{-\pi Y}) \right] \quad \text{as } Y \to \infty.$$
(A51)

We have yet to determine the constant  $\Delta_1$ . To do so, we must proceed to  $O(\varepsilon^2)$  in the fin (A31), where

$$\Omega \frac{\mathrm{d}^2 \Phi_{f2}}{\mathrm{d}Y^2} = -\left. \frac{\partial \Phi_1}{\partial X} \right|_{X=0}, \quad \text{for } Y < 0.$$
 (A52)

The flux on the right-hand side can be evaluated exactly (see Appendix B) given the solution (A50) to give

$$- \frac{\partial \Phi_1}{\partial X} \Big|_{X=0} = \frac{1+c}{\sqrt{e^{-2\pi Y} - 1}}, \quad \text{for } Y < 0.$$
 (A53)

Substituting, and integrating (A52) from Y = 0 to Y < 0 applying (A33), we find the heat flux within the fin

$$-\Omega \frac{d\Phi_{f2}}{dY} = \frac{1+c}{\pi} \tan^{-1} \left( \sqrt{e^{-2\pi Y} - 1} \right), \quad \text{for } Y < 0.$$
 (A54)

In the limit  $Y \to -\infty$ , this gives

$$-\Omega \frac{\mathrm{d}\Phi_{f2}}{\mathrm{d}Y} \to \frac{1+c}{2}, \quad \text{as } Y \to -\infty,$$
 (A55)

which states that the heat flux ((1+c)/2) entering the tip region via conduction up a fin is equal to the heat flux leaving (one half of) the tip region via the fluid ((1+c)/2). This is because all the heat transfer between the fin and fluid occurs in the tip region. Recall that the solution in the fin region is  $\tilde{\phi} = \tilde{\phi}_f = \varepsilon \Delta_1 y + \cdots$ , and substituting  $y = 1 + \varepsilon Y$ , the heat flux along the fin must match with (A55) at  $O(\varepsilon^2)$ , implying that

$$\Delta_1 = -\frac{1+c}{2Q}.\tag{A56}$$

With  $\Delta_1$  determined, the final necessary condition on  $\phi_1$  in the gap region comes from matching with the constant term in (A51), giving

$$\phi_1 = -(1+c)\left(\frac{\log 2}{\pi} + \frac{1}{2\Omega}\right)$$
 at  $y = 1^+$ , (A57)

which closes the problem for  $\phi_1$  – we discuss its solution in § 3.2. This finishes the determination of the temperature field to  $O(\varepsilon)$  throughout the whole domain.

# A.4. Second order in the fin region

The heat flux leaving the tip can also be determined at the next order,  $O(\varepsilon^2)$ , and so can the corresponding temperature correction throughout the entire fin. Although  $\Phi_2$  throughout the tip region is difficult to find, from a global energy balance in that region one can determine the total heat flux leaving the fin,  $\int_{-\infty}^{0} -\partial \Phi_2/\partial X \, dY$ . Then the fin equation (A31) at third order can be integrated and matched with the correction in the fin region. The analysis is given in Appendix C, and the  $O(\varepsilon^2)$  term in the fin region  $(0 \le y < 1, 1-y \gg \varepsilon)$  is

$$\tilde{\phi}_2(y) = \phi_{f2}(y) = \frac{1+c}{4\Omega^2}y,$$
(A58)

which is linear in y, similar to leading order.

# Appendix B. Leading-order heat flux on the fin surface

Calculation of the normal derivative  $\partial W_1/\partial X$  on the fin surface X=0, Y<0, is of interest to the thermal problem in the tip region. In particular, we are interested in the local heat flux out of the fin

$$-\left.\frac{\partial \Phi_1}{\partial X}\right|_{X=0} = \frac{2(1+c)}{c} \left.\frac{\partial W_1}{\partial X}\right|_{X=0}.$$
 (B1)

The solution for  $W_1$  is determined as the imaginary part of a function h(Z), given by

$$h(Z) = \frac{c}{2\pi i} \log \left[ \frac{e^{i\pi/4} - \tan^{1/2}(\pi Z/2)}{e^{i\pi/4} + \tan^{1/2}(\pi Z/2)} \right].$$
 (B2)

Note that, by the Cauchy-Riemann relations

$$\frac{\partial W_1}{\partial X} = \frac{\partial}{\partial X} \text{Im}[h(Z)] = -\frac{\partial}{\partial Y} \text{Re}[h(Z)], \tag{B3}$$

but

$$-\text{Re}[h(Z)] = -\frac{c}{2\pi} \text{Arg} \left[ \frac{-\tan^{1/2}(\pi Z/2) + e^{i\pi/4}}{\tan^{1/2}(\pi Z/2) + e^{i\pi/4}} \right], \tag{B4}$$

where  $Arg(z) \in (-\pi, \pi]$  is the principal argument. Restricting ourselves to the fin surface,  $Z = -i\tilde{Y}$  with  $\tilde{Y} < 0$ 

$$-\text{Re}[h(Z)]|_{X=0} = -\frac{c}{2\pi} \text{Arg} \left[ \frac{1 - \tanh(\pi \tilde{Y}/2) + 2i \tanh^{1/2}(\pi \tilde{Y}/2)}{\tanh(\pi \tilde{Y}/2) + 1} \right].$$
 (B5)

To evaluate the argument, we note that the term in square brackets always lies in the first quadrant, and hence

$$-\text{Re}[h(Z)]|_{X=0} = -\frac{c}{2\pi} \tan^{-1} \left( \frac{2 \tanh^{1/2}(\pi \tilde{Y}/2)}{1 - \tanh(\pi \tilde{Y}/2)} \right).$$
 (B6)

Taking  $\partial/\partial Y = -\partial/\partial \tilde{Y}$  of the above, we arrive at

$$\frac{\partial W_1}{\partial X}\Big|_{X=0} = \frac{c/2}{\sqrt{e^{2\pi}\tilde{Y} - 1}} = \frac{c/2}{\sqrt{e^{-2\pi Y} - 1}} \quad \text{for } Y < 0.$$
 (B7)

Finally, from (A50), the  $O(\varepsilon)$  heat flux out of the fin follows via

$$-\left.\frac{\partial \Phi_1}{\partial X}\right|_{X=0} = \frac{2(1+c)}{c} \left.\frac{\partial W_1}{\partial X}\right|_{X=0} = \frac{1+c}{\sqrt{\mathrm{e}^{-2\pi Y}-1}} \quad \text{for } Y < 0.$$
 (B8)

# Appendix C. Second order in the tip and fin regions

# C.1. Second-order heat flux from the fin tips

The second-order temperature  $\Phi_2$  in the tip region, although useful, is likely significantly more difficult to find than  $\Phi_1$ . This is due to a non-uniform Dirichlet condition appearing on the fin surface (see below). Consequently, we do not attempt to calculate here the local heat flux correction on the fin,  $(\partial \Phi_2/\partial X)|_{X=0}$ . However, the total heat flux leaving the fin in the tip region, i.e.  $\int_{-\infty}^{0} (\partial \Phi_2/\partial X)|_{X=0} dY$ , is desirable and can be easily extracted without detailed knowledge of  $\Phi_2$  (For the case of infinitely conducting fins,  $\Omega = \infty$ , the  $\Phi_2$  problem reduces to one similar to that of  $W_0$ , and hence can be shown to be identically zero,  $\Phi_2 \equiv 0$ ). The problem for  $\Phi_2$  follows from (A28), (A29), (A32) as

$$\nabla_{XY}^2 \Phi_2 = 0 \quad \text{in } \mathcal{D}_{tip}, \tag{C1}$$

$$\frac{\partial \Phi_2}{\partial X} = 0 \quad \text{on } X = 0, 1, \quad 0 < Y,$$

$$\Phi_2 = \Phi_{f2} \quad \text{on } X = 0, 1, \quad Y < 0,$$
(C2)

$$\Phi_2 = \Phi_{f2}$$
 on  $X = 0, 1, Y < 0,$  (C3)

along with (A54) determining  $\Phi_{f2}$ . We express the matching conditions in terms of heat fluxes. The heat flux entering the gap region is completely satisfied at leading order, (A45), hence all higher orders must have no heat flux, giving

$$\frac{\partial \Phi_2}{\partial Y} \to 0 \quad \text{as } Y \to \infty.$$
 (C4)

The heat flux in the fluid leaving the top of the fin region  $(y \to 1^-)$  is given by  $\partial \tilde{\phi}/\partial y = \varepsilon \Delta_1 + \cdots$ , resulting in the matching condition for  $\Phi_2$ 

$$\frac{\partial \Phi_2}{\partial Y} \to \Delta_1 \quad \text{as } Y \to -\infty.$$
 (C5)

As  $\Phi_2$  is harmonic with known Neumann conditions along the entire boundary of  $\mathcal{D}_{tip}$  except the fins, we may integrate (C1) over  $\mathcal{D}_{tip}$  and apply the divergence theorem. The only non-zero contributions from the boundary are from the fins, and the fluid as  $Y \to -\infty$ 

$$2\int_0^{-\infty} \left. \frac{\partial \Phi_2}{\partial X} \right|_{X=0} dY + \int_0^1 \left. -\frac{\partial \Phi_2}{\partial Y} \right|_{Y\to -\infty} dX = 0.$$
 (C6)

The second term is known from (C5), thus the total heat flux correction from the fin in the tip region is

$$-\int_{-\infty}^{0} \left. \frac{\partial \Phi_2}{\partial X} \right|_{X=0} dY = \frac{\Delta_1}{2} = -\frac{1+c}{4\Omega}.$$
 (C7)

C.2 Second order temperature in the fin region: 0 < y < 1

We have found the leading order solution  $\tilde{\phi} = \varepsilon \Delta_1 y + \cdots$  in the fin region (0 < y < 1), but it is now straightforward to calculate the correction to this at  $O(\varepsilon^2)$ . Looking at  $O(\varepsilon^1)$  in (A1) and  $O(\varepsilon^3)$  in (A6), identical arguments to at lower orders gives that  $\tilde{\phi}_3(y)$  depends only on y, and  $\tilde{\phi}_2(y)$  is linear in y:

$$\tilde{\phi}_2(y) = \phi_{f2}(y) = \Delta_2 y, \quad \text{for } 0 < y < 1,$$
 (C8)

where  $\Delta_2$  is a constant, which we determine via an integration argument in the tip region, similar to how  $\Delta_1$  was determined at the previous order. First, substituting  $y = 1 + \varepsilon Y$  into the fin temperature  $\phi_f = \varepsilon \Delta_1 y + \varepsilon^2 \Delta_2 y + \cdots$  and taking d/dY, we find

$$\frac{\mathrm{d}\phi_f}{\mathrm{d}V} = \varepsilon^2 \Delta_1 + \varepsilon^3 \Delta_2 + \cdots, \tag{C9}$$

which, matching with the fin temperature in the tip region as  $Y \to -\infty$ , gives the condition at *third order* 

$$\frac{\mathrm{d}\Phi_{f3}}{\mathrm{d}Y} \to \Delta_2 \quad \text{as } Y \to -\infty. \tag{C10}$$

The equation for  $\Phi_{f3}$  is given by (A31) at  $O(\varepsilon^2)$ , and integrating it from Y = 0 to  $Y = -\infty$ , applying the no-flux condition at the tip Y = 0,

$$\lim_{Y \to -\infty} \Omega \frac{\mathrm{d}\Phi_{f3}}{\mathrm{d}Y} = \int_{-\infty}^{0} \left. \frac{\partial \Phi_{2}}{\partial X} \right|_{X=0} \mathrm{d}Y. \tag{C11}$$

But the limit on the left hand side equals  $\Delta_2$  from matching, (C10), and the right hand side was already determined to be  $-\Delta_1/2$  in (C7). Hence,

$$\Delta_2 = -\frac{\Delta_1}{2\Omega} = \frac{1+c}{4\Omega^2},\tag{C12}$$

and the correction in the fin region is finally

$$\tilde{\phi}_2(y) = \phi_{f2}(y) = \frac{1+c}{4\Omega^2}y.$$
 (C13)

#### T.L. Kirk and M. Hodes

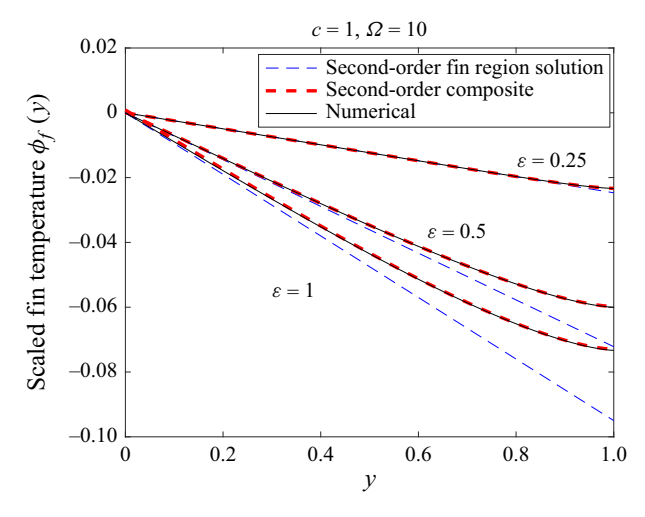


Figure 12. Comparison of the composite solution for the (scaled) temperature in the fin, given by (C18), with the numerical solution.

# C.3. Second-order composite fin temperature

We can now determine a composite solution for the temperature throughout the fin, accurate to  $O(\varepsilon^2)$ . Integrating (A54) from Y = 0 (the tip) to Y < 0

$$\Phi_{f2}(Y) = \Phi_{f2}(0) + \frac{(1+c)}{\pi \Omega} \int_{Y}^{0} \tan^{-1} \left( \sqrt{e^{-2\pi Y'} - 1} \right) dY',$$
(C14)

which can be shown to have asymptotic behaviour as  $Y \to -\infty$ 

$$\Phi_{f2}(Y) \sim \Phi_{f2}(0) - \frac{(1+c)}{2\Omega} \left( Y + \frac{\log 2}{\pi} \right) + o(1).$$
(C15)

Matching with the fin region solution  $\phi_f = \varepsilon \Delta_1 + \varepsilon^2 (\Delta_1 Y + \Delta_2) + \cdots$  as  $Y \to 0$  implies

$$\Phi_{f2}(0) - \frac{(1+c)\log 2}{2\Omega} = \frac{1+c}{4\Omega^2},$$
(C16)

determining  $\Phi_{f2}(0)$ . Then a second-order tip–fin composite  $(0 \leqslant y \leqslant 1)$  is given by

$$\phi_{f,comp} = \varepsilon \Phi_{f1} + \varepsilon^2 \Phi_{f2}(Y) + \varepsilon \phi_{f1}(y) + \varepsilon^2 \phi_{f2}(y) + \underbrace{\frac{\varepsilon(1+c)}{2\Omega}(1+\varepsilon Y) - \frac{\varepsilon^2(1+c)}{4\Omega^2}}_{-\text{overlap}},$$

$$= -(1+c) \left[ \frac{\varepsilon}{2\Omega} - \frac{\varepsilon^2 y}{4\Omega^2} - \frac{\varepsilon^2}{2\Omega} \left( \frac{\log 2}{\pi} + \frac{2}{\pi} \int_{(y-1)/\varepsilon}^{0} \tan^{-1} \sqrt{e^{-2\pi Y'} - 1} \, dY' \right) \right].$$
(C18)

A comparison of  $\phi_{f,comp}$  and the numerical solution is shown in figure 12, and the deviation of the temperature from linear is captured well.

# Appendix D. Solution method for $\hat{\lambda}_1$ and $\hat{\phi}_1$

The problem for the correction in the gap region, 1 < y < 1 + c (or  $0 < \hat{y} < 1$  in transformed coordinates) is given by (3.38)–(3.41). After substituting  $\hat{\lambda}_1$ , given by (3.41), into the  $\hat{\phi}_1$  equation (3.38), and rearranging slightly, the problem can be written in the form

$$\mathcal{L}_1[\hat{\phi}_1] = \hat{\lambda}_0 \widehat{\mathcal{W}}_1 \hat{\phi}_0 - \hat{\lambda}_0^2 \widehat{\mathcal{W}}_0 \hat{\phi}_0 \int_0^1 \widehat{\mathcal{W}}_1 \hat{\phi}_0 \, \mathrm{d}\hat{y} \quad \text{in } 0 < \hat{y} < 1, \tag{D1}$$

$$\frac{d\hat{\phi}_1}{d\hat{y}} = 0 \qquad \text{on } \hat{y} = 1, \tag{D2}$$

$$\hat{\phi}_1 = -\left(\frac{\log 2}{\pi} + \frac{1}{2\Omega}\right) \quad \text{on } \hat{y} = 0, \tag{D3}$$

where the linear (integro-differential) operator  $\mathcal{L}_1$  operating on  $\hat{\phi}_1$  is

$$\mathcal{L}_{1}[\phi] = \frac{\mathrm{d}^{2}\phi}{\mathrm{d}\hat{v}^{2}} - \hat{\lambda}_{0}\widehat{\mathcal{W}}_{0}\phi + \hat{\lambda}_{0}^{2}\widehat{\mathcal{W}}_{0}\hat{\phi}_{0} \int_{0}^{1}\widehat{\mathcal{W}}_{0}\phi\,\mathrm{d}\hat{y},\tag{D4}$$

and the forcing appearing on the right-hand side of (D1) is known. This linear problem has two inhomogeneities: one in the governing equation (D1) and one in the boundary condition (D3) on  $\hat{y} = 0$ . Hence, we can satisfy each inhomogeneity separately and linearly superimpose the corresponding solutions. In particular, if we find a  $\phi^A$  that satisfies the inhomogeneous (normalised) boundary condition but homogeneous equation, given by

$$\mathcal{L}_1[\phi^A] = 0, \quad \text{in } 0 < \hat{y} < 1,$$
 (D5)

$$\frac{\mathrm{d}\phi^A}{\mathrm{d}\hat{\mathbf{v}}} = 0 \qquad \text{on } \hat{\mathbf{y}} = 1, \tag{D6}$$

$$\phi^A = -1 \qquad \text{on } \hat{y} = 0, \tag{D7}$$

and a  $\phi^B$  that satisfies the homogeneous boundary condition but inhomogeneous equation, given by

$$\mathcal{L}_1[\phi^B] = \hat{\lambda}_0 \widehat{\mathcal{W}}_1 \hat{\phi}_0 - \hat{\lambda}_0^2 \widehat{\mathcal{W}}_0 \hat{\phi}_0 \int_0^1 \widehat{\mathcal{W}}_1 \hat{\phi}_0 \, \mathrm{d}\hat{y}, \quad \text{in } 0 < \hat{y} < 1, \tag{D8}$$

$$\frac{\mathrm{d}\phi^B}{\mathrm{d}\hat{\mathbf{y}}} = 0 \qquad \text{on } \hat{\mathbf{y}} = 1, \tag{D9}$$

$$\phi^B = 0 \qquad \text{on } \hat{y} = 0, \tag{D10}$$

then the solution for  $\hat{\phi}_1$  we desire is

$$\hat{\phi}_1 = \left(\frac{\log 2}{\pi} + \frac{1}{2\Omega}\right)\phi^A + \phi^B. \tag{D11}$$

The solution for  $\hat{\lambda}_1$  follows from (3.41)

$$\hat{\lambda}_1 = -\hat{\lambda}_0^2 \left[ \left( \frac{\log 2}{\pi} + \frac{1}{2\Omega} \right) \int_0^1 \widehat{\mathcal{W}}_0 \phi^A \, \mathrm{d}\hat{y} + \int_0^1 \widehat{\mathcal{W}}_0 \phi^B \, \mathrm{d}\hat{y} + \int_0^1 \widehat{\mathcal{W}}_1 \hat{\phi}_0 \, \mathrm{d}\hat{y} \right], \quad (D12)$$

or after rearranging

$$\hat{\lambda}_1 = b_0 + \frac{b_1}{2\Omega},\tag{D13}$$

where

$$b_0 = -\hat{\lambda}_0^2 \left[ \frac{\log 2}{\pi} \int_0^1 \widehat{\mathcal{W}}_0 \phi^A \, d\hat{y} + \int_0^1 \widehat{\mathcal{W}}_0 \phi^B \, d\hat{y} + \int_0^1 \widehat{\mathcal{W}}_1 \hat{\phi}_0 \, d\hat{y} \right], \tag{D14}$$

$$b_1 = -\hat{\lambda}_0^2 \int_0^1 \widehat{\mathcal{W}}_0 \phi^A \, \mathrm{d}\hat{y}. \tag{D15}$$

Given the solutions  $\phi^A$ ,  $\phi^B$  and the leading-order solution  $\hat{\lambda}_0$ ,  $\hat{\phi}_0$ , the above quantities  $b_0$ ,  $b_1$  are easily computed and have no parameters, therefore they are simply numerical constants that only need to be computed once. To do so, we use the same Chebyshev collocation methods used to compute  $\hat{\lambda}_0$ , but here note that the problems for  $\phi^A$  and  $\phi^B$  are both linear and iteration is unnecessary, with  $b_0$ ,  $b_1$  computed afterwards. Mesh refinement was performed by doubling the number of grid points until the relative change in  $b_0$  and  $b_1$  were both less than  $10^{-4}$ . The final values are given by (3.43).

# Appendix E. Problem in the tip region when $c \sim \varepsilon$

Here, we briefly describe the thermal problem when c becomes comparable to  $\varepsilon$  and the asymptotic solutions in the main body of the paper break down. The chief modifications occur in the tip region,  $y-1=O(\varepsilon)$ , where now the top wall is only a distance  $c=O(\varepsilon)$ away. Define  $\hat{c} = c/\varepsilon = O(1)$  as  $\varepsilon \to 0$ . Then Miyoshi et al. (2024) considered the hydrodynamic problem for this case.

#### E.1. Flow problem

In the hydrodynamic problem, the fin region  $(0 < y, 1 - y \gg \varepsilon)$  is unaffected, and the flow is  $O(\varepsilon^2)$  and takes the form  $\tilde{w} = \varepsilon^2 X(1-X)/2 + \cdots$ . However, in the tip region,  $(y-1)/\varepsilon = Y = O(1)$ , we now have a semi-infinite strip,  $\mathcal{D}_{tip} = \{0 < X < 1, -\infty < 1\}$  $Y \leq \hat{c}$ , in which the flow problem w = W(X, Y) is

$$\nabla_{XY}^2 W = -\varepsilon^2 \qquad \text{in } \mathcal{D}_{tip}, \tag{E1}$$

$$W = 0$$
 on  $X = 0, 1, Y < 0,$  (E2)

$$\nabla_{XY}^{2}W = -\varepsilon^{2} \quad \text{in } \mathcal{D}_{tip},$$

$$W = 0 \quad \text{on } X = 0, 1, \quad Y < 0,$$

$$\frac{\partial W}{\partial X} = 0 \quad \text{on } X = 0, 1, \quad 0 < Y < \hat{c},$$
(E1)

with now no slip at  $Y = \hat{c}$ , and matching with Poiseuille flow as  $Y \to -\infty$ 

$$W = 0 \qquad \text{on } Y = \hat{c}, \tag{E4}$$

$$W \to \frac{1}{2}\varepsilon^2 X(1-X) + \cdots$$
 as  $Y \to -\infty$ . (E5)

Notice that the flow in this tip region is now  $O(\varepsilon^2)$  (compared with  $\varepsilon$ ), and thus is comparable to the flow in the fin region; indeed the flow is the same order in each region. Writing  $W = \varepsilon^2 W_2 + \cdots$ , then a form of the problem for  $W_2$  was solved by Miyoshi *et al.* (2024) (in different coordinates) with considerable difficulty, employing a conformal map to an annulus. Although, a simpler solution was found in the sub-limit  $\hat{c} \ll 1$ .

# E.2. *Thermal problem*

Moving to the thermal problem in the limit  $\hat{c} = c/\varepsilon = O(1)$ , we now attempt to give estimates for the various terms in the thermal energy equation in the aforementioned regions. First, from the leading-order result (3.44) for  $\lambda$ , if we now consider  $c = O(\varepsilon)$  in that expression we get  $\lambda = O(\varepsilon^{-1})$ . Then from (A10) we estimate  $\phi = O(\varepsilon)$  throughout the fluid.

With these estimates, the problem in the fin region  $(0 < y, 1 - y \gg \varepsilon)$  gives  $\partial \phi / \partial X \equiv 0$  to leading order, i.e.  $\phi \sim \varepsilon \phi_1(y) + \varepsilon^2 \phi_2(X, y) + \cdots$ . Then the leading-order balance in (A1) occurs at O(1), which includes advection and conduction in X

$$\underbrace{\lambda \mathcal{W} \phi}_{O(1)} = \underbrace{\frac{1}{\varepsilon^2} \frac{\partial^2 \phi}{\partial X^2}}_{O(1)} + \underbrace{\frac{\partial^2 \phi}{\partial y^2}}_{O(\varepsilon)},\tag{E6}$$

but not conduction in y, which is of higher order. Hence, there is a local 1-D convection problem, coupled to a conduction problem in the fin.

In the tip region  $((y-1)/\varepsilon = Y = O(1))$ , the problem will be similar, but with  $\phi$  being constant at leading order,  $\phi = \varepsilon C + \varepsilon^2 \phi_2(X, Y)$ . This would lead to a leading-order balance at O(1) again, between advection and conduction in both directions (X and Y)

$$\underbrace{\lambda \mathcal{W} \phi}_{O(1)} = \underbrace{\frac{1}{\varepsilon^2} \frac{\partial^2 \phi}{\partial X^2}}_{O(1)} + \underbrace{\frac{1}{\varepsilon^2} \frac{\partial^2 \phi}{\partial Y^2}}_{O(1)}.$$
 (E7)

It would also apply in a semi-strip, as one would also need to enforce the adiabatic condition at  $Y = \hat{c}$ . The problem in the tip region would be analytically intractible, as the flow there depends on (X, Y).

From the above estimates, we see that advection becomes important (appearing at leading order) throughout the fluid, i.e. in both the fin and tip regions. The main difference between the regions then is only whether conduction is one- or two-dimensional. In our asymptotics for c = O(1) (the main limit of the paper), advection is negligible in both of these regions, instead only appearing in the 'gap region' above. Clearly the breakdown of the solution as c is decreased is largely due to this neglect of advection, which can no longer be avoided when c becomes comparable to  $\varepsilon$ .

#### REFERENCES

CURR, R.M., SHARMA, D. & TATCHELL, D.G. 1972 Numerical predictions of some three-dimensional boundary layers in ducts. *Comput. Meth. Appl. Mech. Engng* **1** (2), 143–158.

GAME, S.E., HODES, M., KIRK, T.L. & PAPAGEORGIOU, D.T. 2018 Nusselt numbers for Poiseuille flow over isoflux parallel ridges for arbitrary meniscus curvature. *J. Heat Transfer* **140** (8), 081701.

IYENGAR, M. & BAR-COHEN, A. 2007 Design for manufacturability of forced convection air cooled fully ducted heat sinks. *Electronics Cooling* 13 (3), 12.

KARAMANIS, G. 2015 Optimized longitudinal-fin heat sinks accounting for nonuniform heat transfer coefficients, Master's thesis. Tufts University.

KARAMANIS, G. & HODES, M. 2016 Longitudinal-fin heat sink optimization capturing conjugate effects under fully developed conditions. *J. Therm. Sci. Engng Appl.* 8 (4), 041011.

KARAMANIS, G. & HODES, M. 2019a Conjugate nusselt numbers for simultaneously developing flow through rectangular ducts. J. Heat Transfer 141 (8), 081701.

KARAMANIS, G. & HODES, M. 2019b Simultaneous optimization of an array of heat sinks. J. Electron. Packag. 141 (2), 021001.

MARTIN, E., VALEIJE, A., SASTRE, F. & VELAZQUEZ, A. 2022 Impact of channels aspect ratio on the heat transfer in finned heat sinks with tip clearance. *Micromachines-BASEL* 13 (4), 599.

#### T.L. Kirk and M. Hodes

- MAYER, M.D., KADOKO, J. & HODES, M. 2021 Two-dimensional numerical analysis of gas diffusion-induced Cassie to Wenzel state transition. *J. Heat Transfer* **143** (10), 103001.
- MIYOSHI, H., KIRK, T.L., HODES, M. & CROWDY, D.G. 2024 Fully developed flow through shrouded-fin arrays: exact and asymptotic solutions. *J. Fluid Mech.* **991**, A2.
- REYES, M., ARIAS, J.R., VELAZQUEZ, A. & VEGA, J.M. 2011 Experimental study of heat transfer and pressure drop in micro-channel based heat sinks with tip clearance. *Appl. Therm. Engng* **31** (5), 887–893.
- SHAH, R.K. & LONDON, A.L. 1978 Laminar Flow Forced Convection in Ducts: A Source Book for Compact Heat Exchanger Analytical Data. Academic Press.
- SPARROW, E.M., BALIGA, B.R. & PATANKAR, S.V. 1978 Forced convection heat transfer from a shrouded fin array with and without tip clearance. *J. Heat Transfer* **100** (4), 572–579.
- Sparrow, E.M. & Hsu, C.F. 1981 Analytically determined fin-tip heat transfer coefficients. *J. Heat Transfer* **103** (1), 18–25.
- SPARROW, E.M. & KADLE, D.S. 1986 Effect of tip-to-shroud clearance on turbulent heat transfer from a shrouded, longitudinal fin array. *J. Heat Transfer* **108** (3), 519–524.
- SUN, P., ISMAIL, M.A. & MUSTAFFA, A.F. 2025 Metamodel-based design optimization for heat transfer enhancement of finned heat sinks. *Intl J. Therm. Sci.* 214, 109896.
- TREFETHEN, L.N. 2000 Spectral methods in MATLAB. SIAM.
- ZHANG, R., HODES, M., LOWER, N. & WILCOXON, R. 2015 Water-based microchannel and galinstan-based minichannel cooling beyond 1 kw cm<sup>-2</sup> heat flux. *IEEE Trans. Compon. Packag. Manufacturing Technol.* **5** (6), 762–770.